Transmembrane Proteins UNC-40/DCC, PTP-3/LAR, and MIG-21 Control Anterior–Posterior Neuroblast Migration with Left–Right Functional Asymmetry in *Caenorhabditis elegans*

Lakshmi Sundararajan and Erik A. Lundquist[1]
Programs in Genetics and Molecular, Cellular, and Developmental Biology, Department of Molecular Biosciences, University of Kansas, Lawrence, Kansas 66045

ABSTRACT Migration of neurons and neural crest cells is of central importance to the development of nervous systems. In *Caenorhabditis elegans*, the QL neuroblast on the left migrates posteriorly, and QR on the right migrates anteriorly, despite similar lineages and birth positions with regard to the left–right axis. Initial migration is independent of a Wnt signal that controls later anterior–posterior Q descendant migration. Previous studies showed that the transmembrane proteins UNC-40/DCC and MIG-21, a novel thrombospondin type I repeat containing protein, act redundantly in left-side QL posterior migration. Here we show that the LAR receptor protein tyrosine phosphatase PTP-3 acts with MIG-21 in parallel to UNC-40 in QL posterior migration. We also show that in right-side QR, the UNC-40 and PTP-3/MIG-21 pathways mutually inhibit each other's role in posterior migration, allowing anterior QR migration. Finally, we present evidence that these proteins act autonomously in the Q neuroblasts. These studies indicate an inherent left–right asymmetry in the Q neuroblasts with regard to UNC-40, PTP-3, and MIG-21 function that results in posterior *vs.* anterior migration.

CELL migration is a fundamental event in the development of nervous systems. In the vertebrate central nervous system, neurons and neuroblasts migrate radially to populate distinct layers in the cerebellar and cerebral cortices, and neural crest cells migrate along distinct paths in the vertebrate embryo to give rise to the peripheral nervous system. The Q neuroblasts in *Caenorhabditis elegans* are a useful model to study the migration of neuroblasts and neurons in the anterior–posterior axis. The Q neuroblasts are a bilaterally symmetric pair of cells in the posterior–lateral region of the animal, with QR on the right side and QL on the left side (Sulston and Horvitz 1977). The Q neuroblasts are born in embryogenesis and are the sisters of the V5 hypodermal seam cells. By 5 hr after hatching, QR has migrated anteriorly and divided over the V4 seam cell, and QL has migrated posteriorly and divided over the V5 seam cell (Honigberg and Kenyon 2000; Chapman *et al.* 2008; Dyer *et al.* 2010). The resulting Q cell descendants then undergo a pattern of migration, division, and programmed cell death resulting in three neurons each (AQR, SDQR, and AVM on the right from QR; and PQR, SDQL, and PVM on the left from QL) (Sulston and Horvitz 1977; Chalfie and Sulston 1981). The QR descendant AQR migrates the longest distance to a region near the anterior deirid ganglion in the head, and the QL descendant PQR migrates the longest distance posteriorly to the phasmid ganglion in the tail (Sulston and Horvitz 1977; White *et al.* 1986; Chapman *et al.* 2008). The posterior migration of QL descendants requires the activity of the MAB-5/Hox transcription factor, expression of which is induced in QL descendants by an EGL-20/Wnt signal emanating from the posterior (Chalfie *et al.* 1983; Kenyon 1986; Salser and Kenyon 1992; Harris *et al.* 1996; Whangbo and Kenyon 1999; Korswagen *et al.* 2000; Herman 2003; Eisenmann 2005). QR migrates anteriorly and does not normally receive this EGL-20/Wnt signal, and thus does not express MAB-5/Hox.

The initial anterior and posterior migrations of the QR and QL neuroblasts do not depend on MAB-5 or EGL-20/Wnt

doi: 10.1534/genetics.112.145706
Manuscript received September 7, 2012; accepted for publication October 3, 2012
Supporting information is available online at http://www.genetics.org/lookup/suppl/doi:10.1534/genetics.112.145706/-/DC1/.
[1]Corresponding author: 1200 Sunnyside Ave., 5049 Haworth Hall, University of Kansas, Lawrence, KS 66045. E-mail: erikl@ku.edu

(Chapman *et al.* 2008), as QL and QR protrude and polarize normally in *mab-5* and *egl-20* mutants. While initial Q migration is independent of EGL-20/Wnt, the five *Wnt* genes are involved in subsequent Q descendant guidance along the anterior–posterior axis (Pan *et al.* 2006; Harterink *et al.* 2011; Zinovyeva *et al.* 2008).

The initial Q migrations can affect subsequent MAB-5 expression in the Q descendants (Chapman *et al.* 2008; Middelkoop *et al.* 2012). The extent of posterior protrusion correlates with *mab-5* expression, with more *mab-5* expression in cells that protrude posteriorly (Middelkoop *et al.* 2012), consistent with exposure to the posterior EGL-20/Wnt signal. QR is inherently less sensitive to the EGL-20/Wnt signal than QL (Whangbo and Kenyon 1999; Middelkoop *et al.* 2012), a difference that seems to be mediated by the MIG-21 molecule (*i.e.*, in *mig-21* mutants the differential sensitivity is abolished) (Middelkoop *et al.* 2012).

Previous studies have revealed mechanisms of initial Q neuroblast migration that is independent of EGL-20/Wnt and MAB-5/Hox. The transmembrane immunoglobulin superfamily receptor UNC-40/Deleted in Colorectal Cancer (DCC) controls the anterior–posterior protrusion and migration of both QR and QL (Honigberg and Kenyon 2000; Middelkoop *et al.* 2012). UNC-40/DCC is an UNC-6/Netrin receptor that regulates cell and growth cone migrations in the dorsal–ventral axis (Hedgecock *et al.* 1990; Keino-Masu 1996). UNC-6/Netrin is not involved with UNC-40/DCC in anterior–posterior Q migration (Honigberg and Kenyon 2000), nor does it act with UNC-40 in muscle arm extension (Alexander *et al.* 2009), suggesting that UNC-40/DCC might utilize other ligands in these processes.

To identify additional genes that might act with UNC-40 in initial Q protrusion and migration, we conducted a forward genetic screen for mutants with altered migrations of the QL and QR descendant neurons AQR and PQR, with the idea that they might also affect Q protrusion and migration. This screen identified three new mutations in the *mig-21* gene (Du and Chalfie 2001), which encodes a small transmembrane molecule with two extracellular thrombospondin type I domains. MIG-21 was shown previously to affect Q protrusion and migration and Q descendant migration and to control differential sensitivity of QL and QR to the EGL-20/Wnt signal (Du and Chalfie 2001; Middelkoop *et al.* 2012).

A previous screen for Q descendant migration mutants identified *qid-5(mu245)* (Ch'ng *et al.* 2003), which we found caused misdirected AQR and PQR similar to *unc-40* and *mig-21*. We sequenced the genome of a *qid-5(mu245)* strain and discovered that *qid-5(mu245)* is a new and potential null allele of the *ptp-3* gene, which was previously implicated in Q protrusion and migration (Williams 2003) and which encodes a LAR-type receptor protein tyrosine phosphatase (Harrington *et al.* 2002; Ackley *et al.* 2005). The *ptp-3* locus encodes a family of transmembrane molecules characterized by extracellular immunoglobulin and fibronectin type III repeats and two intracellular phosphatase domains. PTP-3/LAR-related molecules are involved in multiple aspects of nervous system development, including axon guidance, neurite development, and synaptic organization (Ackley *et al.* 2005; Johnson *et al.* 2006; Pawson *et al.* 2008; Hofmeyer and Treisman 2009; Wang *et al.* 2012), cell movements in gastrulation (Harrington *et al.* 2002), and germline stem cell maintenance (Srinivasan *et al.* 2012).

Analysis of double and triple mutants involving *unc-40*, *ptp-3*, *and mig-21* revealed distinct interactions in QL *vs.* QR. In QL we found that UNC-40 and MIG-21 act redundantly in posterior migration, similar to a recently published study (Middelkoop *et al.* 2012). We also found that PTP-3 acts in parallel to UNC-40 in QL posterior migration and might act in the same pathway as MIG-21. Surprisingly, we found that the abnormal posterior migration of QR in *ptp-3* and *mig-21* mutants was suppressed by *unc-40*, and vice versa, leading us to speculate that in QR, UNC-40 and a PTP-3/MIG-21 pathway might mutually inhibit each other's role in posterior migration, allowing for anterior migration of QR. Cell-specific rescue and RNAi experiments indicate that MIG-21, UNC-40, and PTP-3 can act cell autonomously in the Q cells to guide Q migrations.

In sum, we have identified three transmembrane molecules, UNC-40, MIG-21, and PTP-3, that control posterior Q cell migration. UNC-40 and MIG-21/PTP-3 act in parallel in QL and act as mutual inhibitors of one another in QR. These novel interactions between UNC-40, PTP-3, and MIG-21, indicate that complex transmembrane receptor interactions guide initial Q cell protrusion and migration, and that, despite apparent bilateral symmetry, QL and QR use inherently distinct mechanisms to guide initial anterior–posterior migration.

Materials and Methods

C. elegans genetics

All experiments were conducted at 20° using standard culture techniques (Sulston and Hodgkin 1988). The following mutations were used: LGI *unc-40(e1430)*, *unc-40(e271)*, *unc-40(n324)*; LGII *ptp-3(mu256)*, *ptp-3(mu245)*, *ptp-3 (ok244)*, *muIs32[mec-4*::*gfp]*; LGIII *mig-21(u787)*, *mig-21 (lq37)*, *mig-21(lq78)*, *mig-21(lq84)*; LGIV *lqIs80[Pscm promoter*::*gfp*::*caax]*; LGV *sid-1(pk3321)*, *lqIs58[Pgcy-32 promoter*::*cfp]*, *ayIs9[Pegl-17*::*gfp]* (Branda and Stern 2000); LG unassigned *lqIs146[Pscm promoter*::*unc-40(RNAi)]*, *lqEx661[Pscm promoter*::*mig-21(RNAi)]*, *lqIs166[Pscm promoter*::*ptp-3(RNAi)]*; *lqIs151[Pscm promoter*::*unc-40(+)*:: *gfp]*, *lqEx637[Pscm promoter*::*ptp-3B(+)*::*gfp)]*, *juIs197 [ptp-3B(+)*::*gfp]*, *lqEx593[mig-21(+)]*, *lqEx712 [Pdpy-7*:: *ptp-3B(+)]*, *lqEx714 [Pegl-17*::*unc-40(+)]*, *lqEx716 [Pegl-17*::*ptp3B(+)]*. Trangenes were constructed by standard gonadal microinjection to produce extrachromosomal arrays and were stably integrated into the genome using standard trimethylpsoralen and ultraviolet light treatment (Mello and Fire 1995).

Isolation of mig-21 alleles and characterization of the mig-21 locus

The *mig-21* alleles *lq37*, *lq78*, and *lq84* were isolated in an EMS screen for new mutations that affect the positions of the Q cell descendants AQR and PQR (E. A. Lundquist, unpublished results). Single nucleotide polymorphism (SNP) mapping was used to assign these mutations to linkage groups as described in Davis *et al.* (2005). Briefly, males from the polymorphic Hawaiian strain CB4856 were mated to hermaphrodites harboring the new mutation in the N2 background, which also contained the *lqIs58 V* and *lqIs80 IV* marker transgenes. Single F_1 heterozygous hermaphrodites were plated singly, and 10–20 F_2 animals with AQR and PQR migration defects (mutant segregants) were subjected to PCR using the SNP primers described in Davis *et al.* (2005). The PCR products were digested with *Dra*I restriction enzyme to detect the SNP. Relative agarose gel electrophoresis band intensities were used to determine which CB4856-associated SNP's were underrepresented in the mutant segregants. *lq37*, *lq78*, and *lq84* all showed linkage to SNP's on LGIII, and each failed to complement each other and *mig-21(u787)* for AQR and PQR defects (data not shown). The *mig-21* locus from each strain was amplified by polymerase chain reaction (PCR), and the PCR products were sequenced to identify the lesions associated with each allele (primer sequences available upon request). *lq37* was a G-to-A transition (position LGIII 5,877,678 WS228) resulting in a C-to-Y missense change; *lq78* was a G-to-A transition (position LGIII 5,877,466 WS228) resulting in a G-to-E missense; and *lq84* was a G-to-A missense (position LGIII 5,877,289 WS228) resulting in an altered 3′ splice site.

A transgene containing the wild-type *mig-21(+)* locus was generated by amplifying and cloning the *mig-21* gene from N2 genomic DNA. This fragment consisted of the entire region from the predicted upstream and downstream genes relative to *F01F1.13* (LGIII 5,878,514 to 5,876,277, WormBase WS229). The region was sequenced to ensure that no mutations had been introduced by PCR. This construct (*lqEx593*) rescued the AQR and PQR migration defects of *mig-21(u787)*.

In an unrelated experiment, the transcriptomes of L1 larvae ~5 hr after hatching were sequenced using next-generation RNA seq on the Illumina Genome Analyzer IIx (GAIIx) platform (Cofactor Genomics, St. Louis). Sequencing reads were mapped to the *C. elegans* reference genome using TopHat (Langmead *et al.* 2009) and visualized using the Integrated Genomics Viewer 2.0.15 (Robinson *et al.* 2011; Thorvaldsdottir *et al.* 2012). The reads that mapped to the *mig-21* locus are shown in Figure S1 and confirmed the gene structure diagrammed in Figure S2. The 3′ end of the gene structure is identical to that described in Middelkoop *et al.* (2012). The 5′ end differed from the Middelkoop *et al.* (2012) prediction, and was confirmed by a transcript sequencing read as shown on WormBase WS229 (read MM454_FPK17YK01AZZNG). The prediction described here contains a predicted N-terminal signal sequence not found in the Middelkoop *et al.* (2012) prediction.

ptp-3(mu245) identification

The previously identified *qid-5(mu245)* mutant affected AQR and PQR migration in a manner similar to *mig-21*. To identify the gene affected by *qid-5(mu245)*, we subjected a strain harboring the mutation (LE2577; *qid-5(mu245) muIs32 II*; *lqIs80 Iv*; *lqIs58 V*) to genome resequencing using the Illumina GAIIx platform (special thanks to O. Hobert and A. Boyanov, Columbia University, New York). LE2577 reads were compared to the *C. elegans* reference genome using MAQgene (Bigelow *et al.* 2009), which also categorized the predicted effects the polymorphisms had on gene structure and function. LE2577 harbored a predicted C-to-A mutation (position LGII 10,995,118 in WS229) that resulted in a premature stop codon in the *ptp-3* gene. *qid-5(mu245)* had been previously mapped to a region of LGII that contains *ptp-3*. *qid-5(mu245)* failed to complement *ptp-3* for AQR and PQR migration defects (data not shown), indicating that *mu245* is an allele of *ptp-3*.

Scoring AQR and PQR migration defects

Defects in AQR and PQR migration were quantified as described previously (Chapman *et al.* 2008). AQR and PQR were assayed using the *gcy-32*::*cfp* transgene *lqIs58* in L4 or young adult animals. Five regions along the anterior–posterior axis of the animal were considered. Position 1 represents the wild-type position of AQR in the anterior deirid ganglion just posterior to the pharynx; position 2 represents a region anterior to the vulva but posterior to the anterior deirid; position 3 represents a region proximal to the vulva (~10 AQR or PQR cell body widths to the anterior and posterior of the vulva); position 4 represents the birthplace of the Q neuroblasts near the posterior deirid ganglion; and position 5 represents the wild-type position of PQR posterior to the anus in the phasmid ganglion. At least 100 animals of each genotype were scored for AQR and PQR position relative to this scale. Only positions 1 and 5, the unambiguous positions of wild-type AQR and PQR, were used in statistical analysis. Significance was determined using Fisher's exact test.

Scoring Q neuroblast migration defects

The protrusion and migration of the Q neuroblasts was quantified as described previously (Chapman *et al.* 2008). To synchronize animals, adults and larvae were washed from plates, leaving behind eggs. At one-half-hour time points, newly hatched larvae were washed from these plates and allowed to develop on freshly seeded NGM plates. Q cells were analyzed at 2, 3, and 4 hr after synchronization. At 2–2.5 hr posthatch, the Q neuroblasts extend anterior (QR) and posterior (QL) protrusions. By 3–3.5 hr, the Q neuroblasts have migrated above their respective seam cells (V4 for QR; V5 for QL). At 4–4.5 hr, the Q neuroblasts undergo their first division above the seam cells. Protrusion at 2–2.5 hr was scored as anterior if the cell protruded over the V4 seam, as no protrusion if it failed to protrude, and posterior if it protruded over the V5 seam cell. Migration at the 3- to

3.5-hr stage was scored as anterior if the Q cells migrated over the V4 seam cell, as migration failure if the Q cells failed to migrate, and as posterior if the Q cells migrated over the V5 seam cell. Position of division at 4–4.5 hr was scored as anterior if the Q cells divided over the V4 seam cell, as between if the Q cells divided between the V4 and V5 seam cells, and posterior if the Q cells divided over the V5 seam cell. At least 25 cells were scored for each genotype, and significance of difference in migration between genotypes was determined by Fisher's exact analysis. Only position of division at 4–4.5 hr was included in Figure 6, but a table with all of the time-point data are included as Table S1.

ptp-3 and unc-40 transgenes

A transgene consisting of the wild-type *ptp-3B* gene and upstream region fused in frame to *gfp* (*juIs197[ptp-3B::gfp]*) (Ackley *et al.* 2005) rescued AQR and PQR defects of *ptp-3 (mu256)*. We amplified the coding region from this construct and placed it behind the *scm* promoter to drive *ptp-3B::gfp* expression specifically in the seam cells and early Q cells (*lqEx637[scm promoter::ptp-3B::gfp]*) (Chapman *et al.* 2008). Primer and plasmid sequences are available upon request. We created an *scm promoter::unc-40::gfp* transgene (*lqIs151[scm promoter::unc-40(+)::gfp]*) by amplifying the *unc-40::gfp* coding region from the previously described *mec-4 promoter::unc-40::gfp* plasmid (Levy-Strumpf and Culotti 2007) and placing it behind the *scm* promoter. The *dpy-7* promoter (Gilleard *et al.* 1997) (LGX: 7,537,743–7,538,087; WS232) was amplified by PCR and placed upstream of *ptp-3B(+)* and the *egl-17* promoter (Branda and Stern 2000; Cordes *et al.* 2006) (LGX: 485,131–489,794; WS232) was amplified by PCR and placed upstream of *unc-40(+)* and *ptp-3B(+)*. The coding regions of these transgenes were sequenced to ensure that no errors had been introduced by PCR.

Transgenic RNA-mediated gene interference (RNAi)

We used a cell-specific transgenic RNAi approach as described previously (Esposito *et al.* 2007). Fragments of the *mig-21*, *unc-40*, and *ptp-3* coding regions were amplified by PCR and inserted behind the *scm* promoter in a plasmid (primer and plasmid sequences available upon request). For each gene, a "sense" and "antisense" orientation relative to the *scm* promoter was isolated. An equimolar mixture of the sense and antisense plasmids was used to construct transgenic animals. These transgenic animals were predicted to express both sense and antisense RNAs driven by the *scm* promoter in the seam cells and Q cells, which was expected to trigger a double-stranded RNA response in these cells (RNAi). Using this approach, *mig-21(RNAi)* phenocopied *mig-21* mutations in AQR and PQR migration. While *ptp-3(RNAi)* and *unc-40(RNAi)* had no effect on their own, they both enhanced the effects of mutations in the other. Transgenes were crossed into the *sid-1(pk3321)* background to test potential dsRNA spreading and systemic effects of the transgenes.

Results

mig-21 allele isolation and the mig-21 locus

In a screen for new mutations with AQR and PQR migration defects, we identified three new mutations, *lq37*, *lq78*, and *lq84*, that caused directional migration defects of both AQR and PQR. These three alleles mapped to linkage group III (see *Materials and Methods*) and failed to complement one another for AQR and PQR migration (data not shown), suggesting they affected the same gene. The *mig-21* gene, which was previously shown to affect Q descendant migrations (Du and Chalfie 2001; Middelkoop *et al.* 2012), resides on linkage group (LG) III. *mig-21(u787)* failed to complement *lq37*, *lq78*, and *lq84* for AQR and PQR migration defects (data not shown), indicating that these mutations were new alleles of *mig-21*.

mig-21 corresponds to the F01F1.13 gene in WormBase (Middelkoop *et al.* 2012). To confirm the *mig-21* locus structure, we sequenced transcripts from early L1 animals using next generation sequencing (RNA seq) (see *Materials and Methods*). From these reads (Supporting Information, Figure S1) and from cDNAs reported on WormBase, a *mig-21* gene structure was determined as depicted in Figures S1 and S2. The 3′ end (exons 2–5) was identical to that reported by Middelkoop *et al.* (2012). The first exon defined by RNA seq in our prediction differed from the first exon of the Middelkoop *et al.* (2012) model (Figure S1), which is upstream and non-overlapping with our first exon. The initiator ATG in the Middelkoop *et al.* (2012) model is 167 bp upstream of our predicted ATG. No RNA seq reads aligned to this 167-bp upstream exon region (Figure S1), indicating that it is not actively transcribed and is not an exon of *mig-21*. A transcript with our predicted structure could be produced by transgenes described in Middelkoop *et al.* (2012), as these included our entire predicted region as well as the 167-bp upstream sequence.

The *mig-21* locus described here can encode a 313-residue type I transmembrane molecule with an N-terminal signal sequence, two predicted extracellular thrombospondin type I domains, a transmembrane domain, and a short cytoplasmic tail with no obvious similarity to other molecules (Figure 1 and Figure S2). This MIG-21 molecule contained a predicted N-terminal signal sequence not found in the Middelkoop *et al.* (2012) prediction, supporting the accuracy of exon 1 in our gene model.

Sequencing of the *mig-21* gene from *lq37*, *lq78*, and *lq84* revealed nucleotide lesions associated with each allele (Figure S1 and Figure 1). *lq37* contained a G-to-A transition resulting in a missense cysteine to phenylalanine change in the first thrombospondin type I domain. *lq78* showed a G-to-A transition resulting in a glycine-to-glutamic acid missense change in an unconserved region of the predicted extracellular domain, and *lq84* harbored a G-to-A transition in the 3′ splice site of the fourth intron. The previously characterized *mig-21(u787)* mutation is G-to-A transition, resulting in a premature stop codon (tryptophan 65).

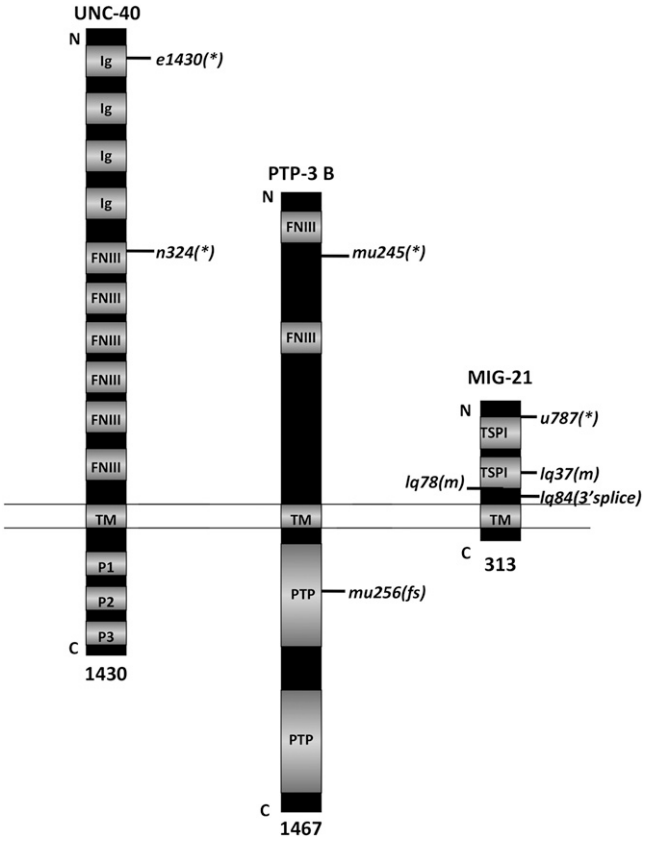

Figure 1 Three transmembrane molecules affect Q neuroblast protrusion and migration. Diagrams of UNC-40/DCC, PTP-3B/LAR, and MIG-21 are shown. The relative positions of nucleotide lesions associated with each mutation used here are indicated. *, nonsense premature stop codon; m, missense mutation; and 3′ splice, the mutation affects the 3′ splice site at that position in the transcript. Ig, immunoglobulin I domain; FNIII, fibronectin type III domain; TM, transmembrane domain; P1, P2, and P3, conserved, proline-rich domains; PTP, protein tyrosine phosphatase domain; TSPI, thrombospondin type I domain.

MIG-21 controls AQR and PQR migration

Our *mig-21* results reported here with the Q cell descendants AQR and PQR migration are similar to those reported in Middelkoop *et al.* (2012), who used the position of the QL.pax and QR.pax neurons (SDQL/R, AVM, and PVM) also derived from QL and QR. AQR and PQR were visualized with a *gcy-32*::*cfp* transgene described previously (Chapman *et al.* 2008). In wild type, the QR descendant AQR on the right migrates anteriorly to the anterior deirid ganglion, and the QL descendant PQR on the left migrates posteriorly to the phasmid ganglion in the tail (Figure 2, A–C). We found that mutations in *mig-21* caused directional defects in both AQR and PQR migration, with PQR affected more strongly (Figures 2 and 3). PQR sometimes migrated anteriorly, and AQR sometimes migrated posteriorly. *mig-21(u787)*, a predicted premature stop codon, was consistently the strongest allele, especially in AQR migration, and is likely a null (Figure 3). The other alleles *lq37*, *lq78*, and *lq84* might be hypomorphic alleles. A transgene harboring a wild-type copy of the *mig-21* locus (see *Materials and Methods*) rescued the AQR and PQR migration defects of *mig-21(u787)* (Figure 3). These results indicate that MIG-21 is involved in determining the direction of AQR and PQR migration.

MIG-21 controls early Q neuroblast migration

Previous results suggested that defects in AQR and PQR migration could be due to earlier defects in the protrusion and migration of the Q neuroblasts from which AQR and PQR are derived (Chapman *et al.* 2008; Dyer *et al.* 2010). We analyzed early Q cell protrusion and migration using the *scm*::*GFP*::*CAAX* reporter gene described previously (Chapman *et al.* 2008; Dyer *et al.* 2010). At 1–1.5 hr posthatching, protrusions start as small filopodial structures that later become large protrusions at 2–2.5 hr after hatching (Figure 4, A–C). QR protrudes anteriorly over the V4 seam cell and QL protrudes posteriorly over V5. At 3–3.5 hr after hatching, the Q cell bodies migrate to reside atop V4 (for QR) and V5 (for QL) (Figure 4, A, D, and E). At 4–4.5 hr after hatching, the Q cells undergo their first division atop the respective seam cells (Figure 4, A, F, and G).

mig-21(u787) and *mig-21(lq37)* mutants displayed defects in the direction of Q neuroblast protrusion (Figure 5, A and B), similar to results in Middelkoop *et al.* (2012). QR sometimes protruded and migrated posteriorly, and QL sometimes protruded and migrated anteriorly. Directional protrusion defects were noted at the first sign of protrusion, suggesting that MIG-21 affects the initial decision about direction of protrusion. We also noted that some protrusions were shorter compared with wild type. *mig-21* Q cell bodies also migrated in the wrong direction and divided atop the incorrect seam cell; QR sometimes migrated posteriorly and divided over V5, and QL sometimes migrated posteriorly and divided over V4. In some cases MIG-21 Q cells failed to migrate (Figure 5F) and divided between the V4 and V5 cells or on their posterior or anterior edges, respectively.

Defects in *mig-21* at the stage of division (4–4.5 hr after hatching) are quantified in Figure 6. QL migration was essentially randomized in both *mig-21(u787)* and *mig-21 (lq37)*, and QR was less severely affected. These data are consistent with Middelkoop *et al.* (2012). We also quantified initial protrusion at 2–2.5 hr and migration at 3–3.5 hr, and similar trends were observed (see Table S1).

UNC-40/DCC controls early Q neuroblast migration

Previous studies have shown that the immunoglobulin superfamily receptor molecule UNC-40/Deleted in Colorectal Cancer controls early Q neuroblast protrusion (Honigberg and Kenyon 2000; Middelkoop *et al.* 2012). We found similar results using the *scm*::*GFP*::*CAAX* reporter to visualize the Q cells (Chapman *et al.* 2008). In *unc-40* mutants, Q cells often initially protruded and migrated in the wrong direction and failed to migrate fully atop the seam cells before dividing (Figures 5E and 6). While similar to *mig-21*, the penetrance of the *unc-40(n324)* and *unc-40(e1430)* phenotypes was consistently lower than those of *mig-21(u787)* and *mig-21(lq37)*.

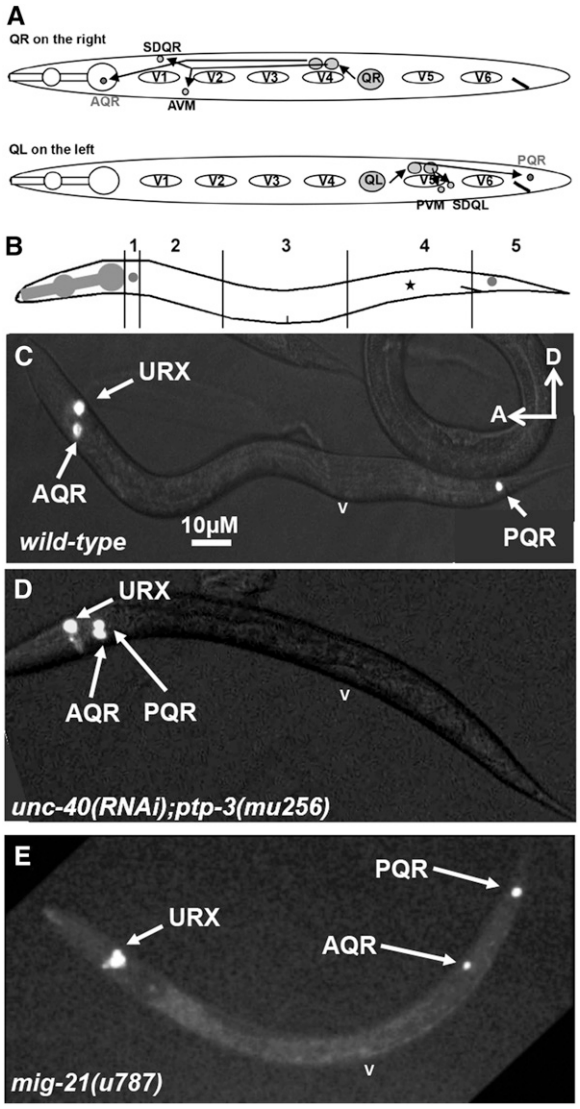

Figure 2 AQR and PQR migration in wild-type and mutants. (A) Simplified diagram of QR and QL migrations and divisions that result in three neurons from each. QR on the right migrates anteriorly above V4 and divides, and the daughters continue anterior migrations and divisions to produce three neurons PQR, SDQR, and AVM. QL on the left migrates posteriorly above V5, divides, and, in response to MAB-5 expression, the daughters continue posterior migration and division to produce PQR, SDQL, and PVM. (B) Diagram showing the scoring positions used in Figures 3 and 7–9 (see *Materials and Methods*). Position 1 is the normal final position of AQR near the anterior deirid ganglion, and position 5 is the normal final position of PQR behind the anus in the phasmid ganglion. The asterisk at position 4 represents the approximate birth place of the Q neuroblasts. Position 3 is proximate to the vulva, and position 2 is anterior to the vulva but still posterior to the anterior deirid ganglion. (C–E) Fluorescent micrographs of animals expressing *cyan fluorescent protein* (*cfp*) from the *gcy-32* promoter in AQR, PQR, and the URXL/R neurons. v, position of the vulva. The scale bar in panel C represents 10 µM for panels C–E. In all micrographs, anterior is to the left, and dorsal is up.

unc-40 also displayed defects in AQR and PQR direction and extent of migration (Figure 3). PQR was more strongly affected than AQR, and the defects were less penetrant than those in *mig-21*. PQR migration defects were significantly less severe in *unc-40(e1430)* compared to *unc-40(n324)*, suggesting that *unc-40(e1430)* might retain some function, although AQR migration and QL/QR migration were not significantly different between *unc-40(e1430)* and *unc-40 (n324)*. A third *unc-40* allele, *e271*, caused defects similar to *unc-40(n324)* that were significantly more severe than *unc-40(e1430)* (Figure 3). Furthermore, the *n324/e1430 trans*-heterozygote resembled *n324* alone (Figure 3). Together, these data suggest that *unc-40(e1430)* is a hypomorph, although it is also possible that *unc-40(e1430)* carries a linked recessive suppressor mutation not found in the other strains.

PTP-3/LAR controls early Q neuroblast migration

To identify other molecules with roles in Q migration similar to MIG-21 and UNC-40, we assayed mutants that had been shown previously to affect Q descendant migrations. *qid-5 (mu245)* was shown to affect the placement of the AVM and PVM Q descendants (Ch'ng *et al.* 2003). We found that *qid-5 (mu245)* also affected AQR and PQR direction and extent of migration similar to *unc-40* and *mig-21*. We used next generation sequencing to determine the genome sequence of a *qid-5(mu245)* strain (see *Materials and Methods*). *qid-5 (mu245)* had been previously mapped to the region of linkage group II (Ch'ng *et al.* 2003), and in this region of the genome we discovered a premature stop codon in the *ptp-3* gene. *ptp-3* had been shown previously to affect Q and descendant migrations (Williams 2003), and we found that *qid-5(mu245)* failed to complement *ptp-3(mu256)* for AQR and PQR migration (data not shown).

The previously described *ptp-3(mu256)* allele is a single nucleotide insertion in the coding region for the first phosphatase domain (Ackley *et al.* 2005) (Figure 1 and Figure S3). *ptp-3(mu245)* introduces a TCA/serine to TAA premature stop at codon 905 in the *ptp-3A* open reading frame and is predicted to affect all known *ptp-3* transcripts except the shortest, *ptp-3C* (Figure 1 and Figure S3). As described below, the *ptp-3B* transcript is the relevant transcript for Q cell migration. *ptp-3B* encodes an isoform of a LAR receptor tyrosine phosphatase-like molecule and consists of an extracellular domain with two fibronectin III repeats, a transmembrane domain, and an intracellular domain with two tyrosine phosphatase domains (Figure 1) (Harrington *et al.* 2002).

Both *ptp-3(mu245)* and *ptp-3(mu256)* caused defects in AQR and PQR migration that resembled *mig-21* and *unc-40* (Figure 3). *ptp-3(mu256)* was shown previously to affect early Q direction and extent of protrusion (Williams 2003), and we found that *ptp-3(mu245)* also affected initial Q direction of protrusion and migration similar to *unc-40* and *mig-21* (Figure 6). The *ptp-3(ok244)* deletion allele affects only a subset of *ptp-3* predicted transcripts with extended 5′ exons (*ptp-3A*, *D*, and *E*; WormBase). *ptp-3(ok244)* caused no defects in AQR or PQR migration (Figure 3) or in early Q neuroblast protrusion and migration (data not shown), suggesting that the *ptp-3A*, *D*, and *E* products are not involved in Q migrations. The *ptp-3B* transcript is the only known

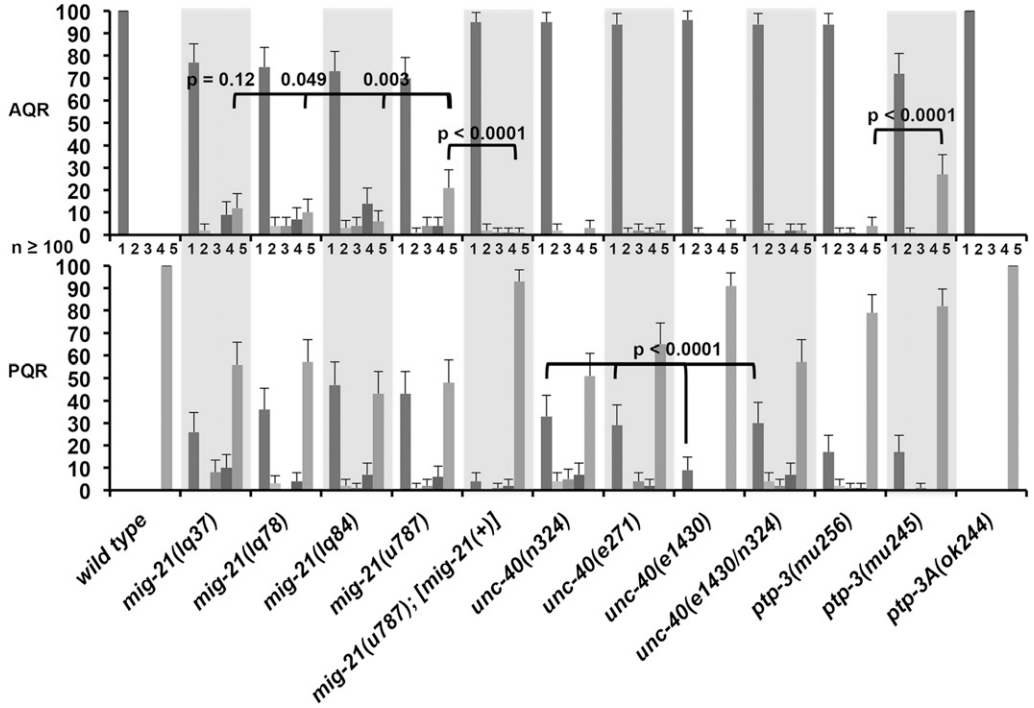

Figure 3 AQR and PQR migration defects in single mutants. The *x*-axis of the graph is the genotype, and the *y*-axis is the percentage of AQR or PQR neurons in each of the five positions (1–5) along the anterior–posterior as described in Figure 2 and *Materials and Methods*. Scale bars represent two times the standard error of the proportion, and significances of difference indicated were determined using the Fisher exact test. At least 100 animals of each genotype were scored.

transcript affected by *mu245* and not affected by *ok244* (Figure S3), suggesting that *ptp-3B* is the relevant isoform in Q and descendant migrations. As shown below, a *ptp-3B* transgene rescued *ptp-3(mu256)*, consistent with this notion.

ptp-3(mu245) displayed significantly more posteriorly directed QR cells and AQR neurons and anterior QL migration than *ptp-3(mu256)* (Figures 3 and 6), suggesting that *ptp-3(mu245)* might be a stronger loss-of-function allele than *ptp-3(mu256)* and might be a null for the affected isoforms, including *ptp-3B*. While *unc-40*, *ptp-3*, and *mig-21* mutations all affected Q and descendant migrations in a similar manner, *mig-21* and *ptp-3* mutants generally had stronger effects than *unc-40* mutants.

MIG-21 and UNC-40 act redundantly in posterior QL migration

mig-21 and *unc-40* mutations both displayed defects in QL posterior protrusion and migration, with some QL cells protruding and migrating to the anterior. *mig-21(u787)*; *unc-40(n324)* double mutants had QL migration defects that were significantly and synergistically more severe than either mutant alone (Figure 6). This phenotypic synergy suggests that UNC-40 and MIG-21 normally act redundantly to control QL posterior migration. These results are consistent with Middelkoop *et al.* (2012), who also found that MIG-21 and UNC-40 redundantly control posterior QL protrusion. The *unc-40(e1430)*; *mig-21(u787)* defects were not significantly different from *mig-21(u787)* alone (Figure 6), supporting the idea that *unc-40(e1430)* is a hypomorph.

PQR migration was also significantly more severely affected in double mutants of two distinct *unc-40 and mig-21* alleles than the single mutants alone (Figure 7). In *unc-40(n324)*; *mig-21(u787)* doubles, the putative double null, only 2% of PQR neurons migrated posteriorly. These results indicate that UNC-40 and MIG-21 redundantly control posterior protrusion and migration of QL and posterior migration of PQR.

Anterior QR migration is regulated through mutual antagonism of MIG-21 and UNC-40

mig-21 and *unc-40* mutants both displayed abnormal posterior protrusion and migration of QR, which normally migrates anteriorly (Figure 6). Surprisingly, *unc-40*; *mig-21* double mutants displayed significantly reduced posterior QR protrusion and migration compared to either single mutant alone (Figure 6). In fact, in no *unc-40*; *mig-21* double mutant scored did we observe a QR that had migrated posteriorly. These data suggest that wild-type UNC-40 activity was required for posterior QR migration in *mig-21* mutants, and that wild-type MIG-21 activity was required for posterior QR migration in *unc-40* mutants. These results imply that in QR, MIG-21 and UNC-40 might normally inhibit the other's role in posterior migration, resulting in the normal anterior migration of QR. When either MIG-21 or UNC-40 is missing, the other is free to drive posterior protrusion and migration.

A similar trend was observed in AQR migration, as significantly fewer AQRs migrated posteriorly in the *unc-40*; *mig-21* double mutants compared to *mig-21* alone (Figure 7). The exception was the *unc-40(e1430)*; *mig-21(lq37)* combination, which was not significantly different from *mig-21(lq37)* alone, again suggesting that *unc-40(e1430)* is a hypomorph.

In sum, these experiments indicate that MIG-21 and UNC-40 are required for posterior Q cell and descendant migration. In QL, MIG-21 and UNC-40 act redundantly to drive posterior protrusion and migration. In QR, MIG-21 and

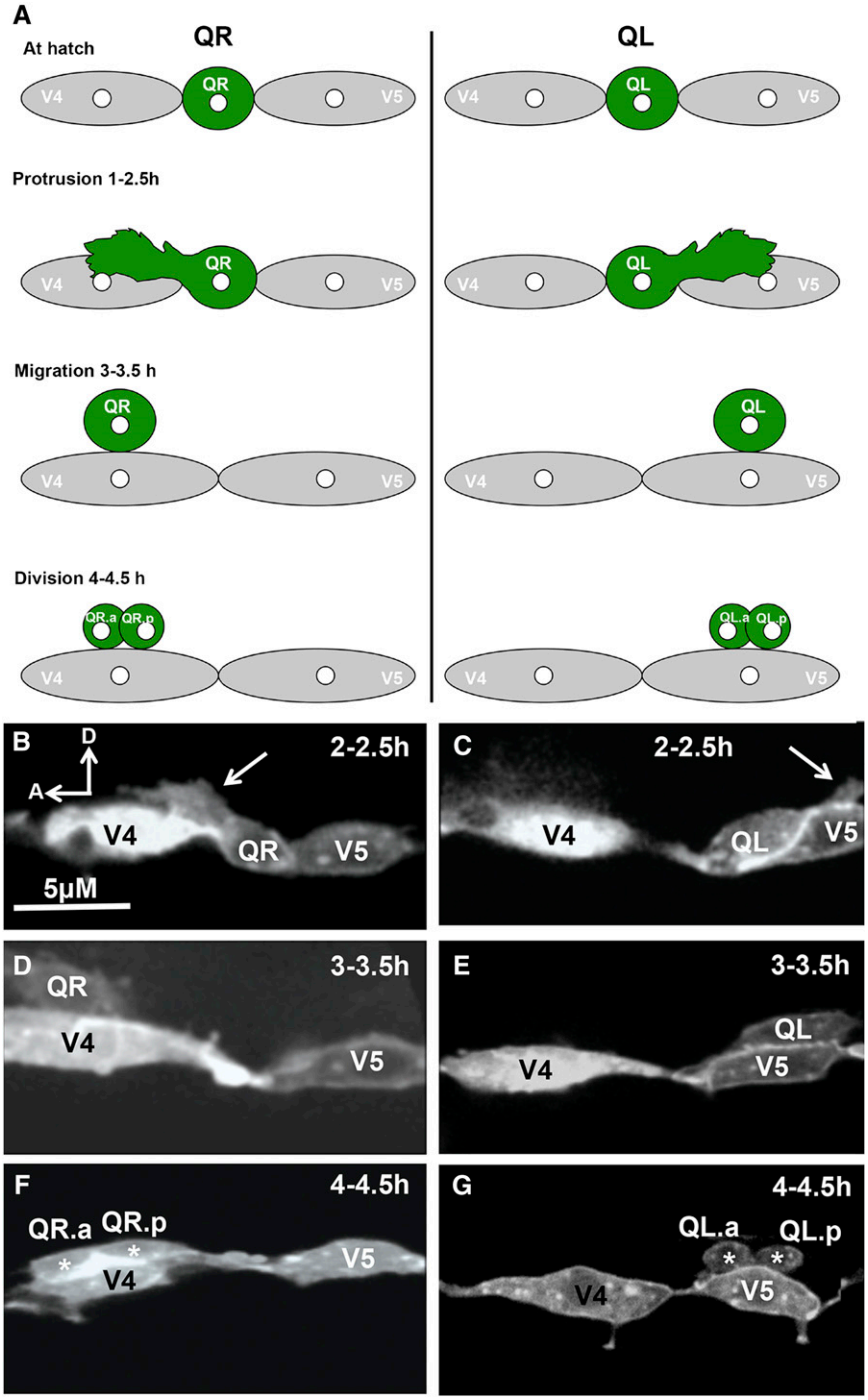

Figure 4 Q neuroblast protrusion and migration in wild type. (A) Diagram of Q neuroblast protrusion and migration, with times after hatching indicated. (B–G) Micrographs of wild-type Q neuroblasts and seam cells V4 and V5 are shown at different stages scored (see *Materials and Methods*). The *Pscm*::*gfp*::*caax* transgene *lqIs80* was used to visualize these cells. In all micrographs, anterior is to the left, and dorsal is up. (B and C) At 2–2.5 hr posthatching, QR sent a protrusion anteriorly over V4 and QL posteriorly over V5 (arrows). (D and E) At 3–3.5 hr, QR had migrated atop V4, and QL had migrated atop V5. (F and G) At 4–4.5 hr, QR had divided above V4 and QL atop V5 (daughter cells denoted by asterisks). Bar (in A), 5 μM for each panel.

UNC-40 might reciprocally inhibit each other, allowing anterior protrusion and migration. In other words, mutation of one revealed a latent ability of QR to protrude and migrate posteriorly, which was dependent on the other.

PTP-3 acts redundantly with UNC-40 in QL, similar to MIG-21

We found that the *unc-40(n324)*; *ptp-3(mu256)* double mutant resulted in embryonic lethality (data not shown), and we were unable to score Q cells and descendants in these mutants. To circumvent this lethality, we used a transgenic RNAi approach to knock down *unc-40* and *ptp-3* in the seam cells and Q cells based on the approach described in Esposito *et al.* (2007) (see *Materials and Methods*). Plasmids were generated to drive expression of sense and antisense RNA complementary to the *unc-40* and *ptp-3* genes under the control of the seam cell promoter (*scm* promoter), which is active in the seam cells and early Q cells (Terns *et al.* 1997; Chapman *et al.* 2008). Animals were made transgenic with a mix of the sense and antisense plasmids, and the resulting transgenes were used in analysis. On their own, *scm*::*ptp-3(RNAi)* and *scm*::*unc-40(RNAi)* lines, from hereon called *ptp-3(RNAi)*

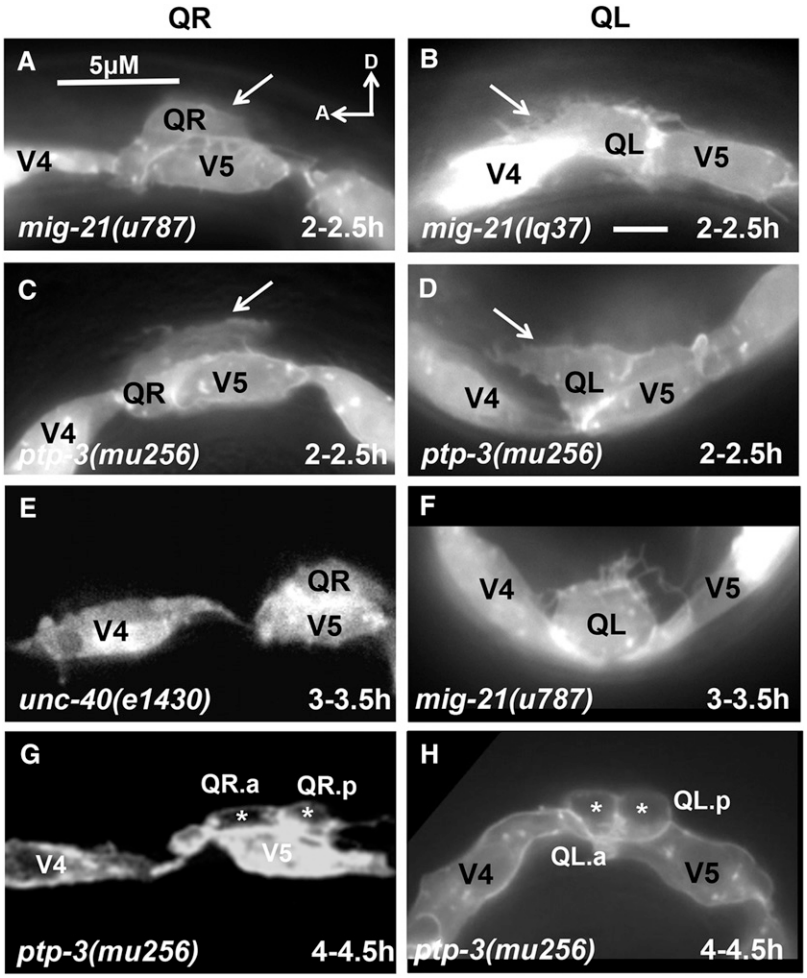

Figure 5 Q neuroblast polarization and migration in mutants. Images are as described in Figure 4, but in different mutant backgrounds. In all micrographs, anterior is to the left, and dorsal is up. (A–C) Images at 2–2.5 hr posthatching. (A) QR neuroblast protruded to the posterior over V5 in *mig-21(u787)* (arrow points to the protrusion). (B) QL neuroblast protruded to the anterior over V4 in a *mig-21(lq37)* mutant (arrow). (C) QR protruded posteriorly over V5 in a *ptp-3(mu256)* mutant. (D) QL protruded anteriorly (arrow). (E and F) Images at 3–3.5 hr posthatching. (E) QR migrated posteriorly atop the V5 seam cell in an *unc-40(e1430)* mutant. (F) QL failed to migrate and resided between V4 and V5 in *mig-21 (u787)*. (G and H) Images at 4–4.5 hr posthatching. (G) QR had divided atop V5 in *ptp-3(mu256)* (daughter cells denoted by asterisks). (H) QL divided between V4 and V5 seam cells in *ptp-3(mu256)*.

and *unc-40(RNAi)*, showed no defects in QR or QL migration (data not shown). However, *unc-40(RNAi)*; *ptp-3(mu256)* and *unc-40(RNAi)*; *ptp-3(mu245)* showed significantly more anterior QL migration compared to *ptp-3(mu256)* and *ptp-3 (mu245)* alone (Figure 6). PQR migration was similarly affected (Figure 7). These results indicate that UNC-40 and PTP-3 act redundantly in QL protrusion and migration. *unc-40(RNAi)* had no effect on its own, indicating that *unc-40 (RNAi)* eliminated some, but not all, *unc-40* activity. *ptp-3 (RNAi)* also had no effect alone but enhanced the PQR migration defects of *unc-40(n324)* (Figure 7). These results indicate that PTP-3 and UNC-40 redundantly control the posterior protrusion and migration of QL and the posterior migration of PQR, similar to MIG-21 and UNC-40.

PTP-3 and UNC-40 display mutual antagonism in QR, similar to MIG-21 and UNC-40

The *unc-40(RNAi)*; *ptp-3(mu245)* double mutant displayed significantly fewer posterior QR and AQR migrations compared to *ptp-3(mu245)* alone (Figures 6 and 7), suggesting mutual antagonism in posterior QR migration as described for UNC-40 and MIG-21. *unc-40(RNAi)* in the *ptp-3(mu256)* hypomorphic background resulted in fewer posterior QR, but this was not statistically significant. This could be due to the fact that neither *unc-40(RNAi)* nor *ptp-3(mu256)* completely eliminates function of either gene, and the hypomorphic *ptp-3(mu256)* had fewer posterior QR/AQR than the null *ptp-3(mu245)*.

In reciprocal experiments targeting *ptp-3* with RNAi, we found that *ptp-3(RNAi)*; *unc-40(n324)* animals showed no posterior AQR migration compared to 3% for *unc-40(n324)* alone (Figure 7). While not statistically significant, this result is consistent with PTP-3 function being required for posterior AQR migration in *unc-40* mutants.

In sum, interactions between *ptp-3* and *unc-40* were similar to those observed between *mig-21* and *unc-40*: redundancy in QL/PQR posterior migration and mutual suppression of posterior QR/AQR migration.

PTP-3 and MIG-21 act in the same genetic pathway

ptp-3; *mig-21* double mutants showed no significant change in percentages of QL and QR that migrated to the posterior compared to single *mig-21(u787)* mutants, suggesting that they act in the same pathway (Figure 6). This is in contrast to *unc-40(n324)*; *mig-21(u787)* double mutants, which strongly synergized in QL, suggesting action in parallel pathways (Figure 6). AQR and PQR defects in *mig-21*; *ptp-3* doubles were also not different from *mig-21* alone (Figure 7). The lack of strong genetic enhancement in *mig-21*; *ptp-3*

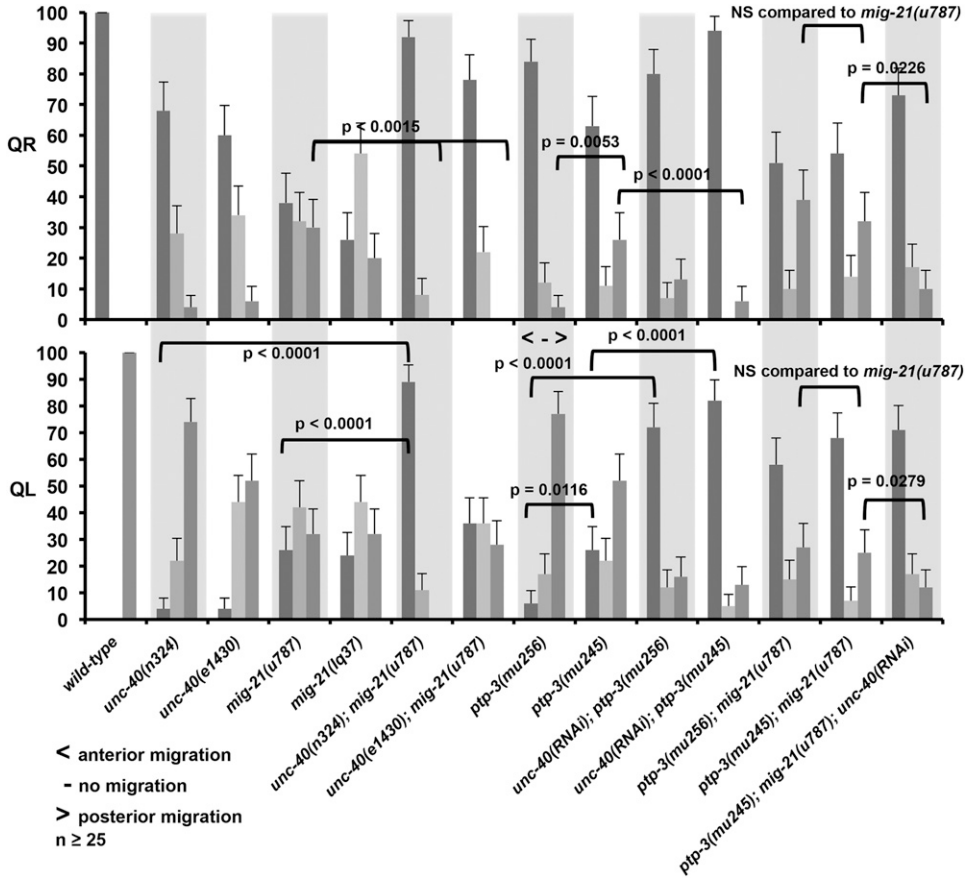

Figure 6 QR and QL migration defects. Graph plots genotype on the *x*-axis against percentage of QR and QL at 4–4.5 hr posthatching that had divided above V4 (anterior migration; bars with dark shading); between V4 and V5 (no migration; bars with light shading); and above V5 (posterior migration; bars with medium shading). Data for the 2- to 2.5-hr protrusion stage and the 3- to 3.5-hr migration stage are included in Supporting Information. The 2- to 2.5-hr and 3- to 3.5-hr data generally follow the trends seen with the 4- to 4.5-hr division stage data shown here. *unc-40(RNAi)* represents the cell-specific *Pscm*::*unc-40(RNAi)* transgene. The error bars represent two times the standard error of the proportion, and significances of difference were calculated by Fisher exact analysis. At least 25 animals were scored for each genotype.

double mutants indicates that PTP-3 and MIG-21 act in the same pathway in Q migrations.

The triple *unc-40(RNAi)*; *ptp-3(mu245)*; *mig-21(u787)* displayed significantly more QL and PQR defects than *ptp-3(mu245)*; *mig-21(u787)*, indicating redundancy between *unc-40* and *ptp-3/mig-21* (Figures 6 and 7). Triple mutant *ptp-3(mu245)*; *mig-21(u787)*; *unc-40(RNAi)* QL and PQR defects were not significantly more severe than *unc-40(n324)*; *mig-21(u787)* or *unc-40(RNAi)*; *ptp-3* doubles (Figures 6 and 7), consistent with MIG-21 and PTP-3 acting in the same pathway in parallel to UNC-40. The *unc-40(RNAi)*; *ptp-3(mu245)*; *mig-21(u787)* triple also displayed significantly fewer posterior QR and AQR migrations than *ptp-3(mu245)*; *mig-21(u787)* (Figures 6 and 7), indicating mutual antagonism of UNC-40 and PTP-3/MIG-21 in QR and AQR posterior migration.

This genetic analysis indicates UNC-40, MIG-21, and PTP-3 all function to promote posterior Q cell and Q descendant migration. IN QL, MIG-21 and PTP-3 act in the same pathway in parallel to UNC-40. In QR, UNC-40 and MIG-21/PTP-3 might define two pathways that mutually antagonize the other's activity in posterior migration, such that anterior migration of these cells can result.

UNC-40, MIG-21, and PTP-3 can act autonomously in the Q cells

We drove the expression of the *unc-40* coding region fused to *green fluorescent protein* (*gfp*) in the seam cells and Q cells using the *scm* promoter (see *Materials and Methods*). This construct was expressed in these cells, and UNC-40::GFP accumulated at the cell margins of the seam cells and Q cells (Figure 8A). Furthermore, *Pscm*::*unc-40*::*gfp* rescued the AQR and PQR migration defects of *unc-40(n324)* (Figure 8D), suggesting that UNC-40 activity in the seam cells and/or Q cells is sufficient for AQR and PQR migration.

We also generated a transgene driving *unc-40* expression in the Q cells and not the seam cells using the *egl-17* promoter (Branda and Stern 2000; Cordes *et al.* 2006). At the time of Q cell migration and division in early L1 (0–6 hr posthatching), the *egl-17* promoter drove *gfp* expression in the Q cells in the posterior, with no detectable expression in other posterior cells (Figure 8C and Middelkoop *et al.* 2012). In the anterior, some pharyngeal cells, the M4 pharyngeal neuron, and a cell that might be the head mesodermal cell expressed *egl-17*::*gfp* (Figure 8C). After Q migration and division (6–10 hr posthatching), *egl-17*::*gfp* expression was detected in the P cells (the vulval precursor cells) in the posterior (data not shown). However, at the time of Q migration, *egl-17*::*gfp* expression was limited to the Q cells in the posterior.

The *Pegl-17*::*unc-40* transgene rescued AQR and PQR migration defects of *unc-40(n324)* (Figure 8D). As the *egl-17* promoter was active only in Q cells in the posterior at the time of Q migration and division, Q cell expression is the most likely source for *unc-40* rescue. Although non-Q

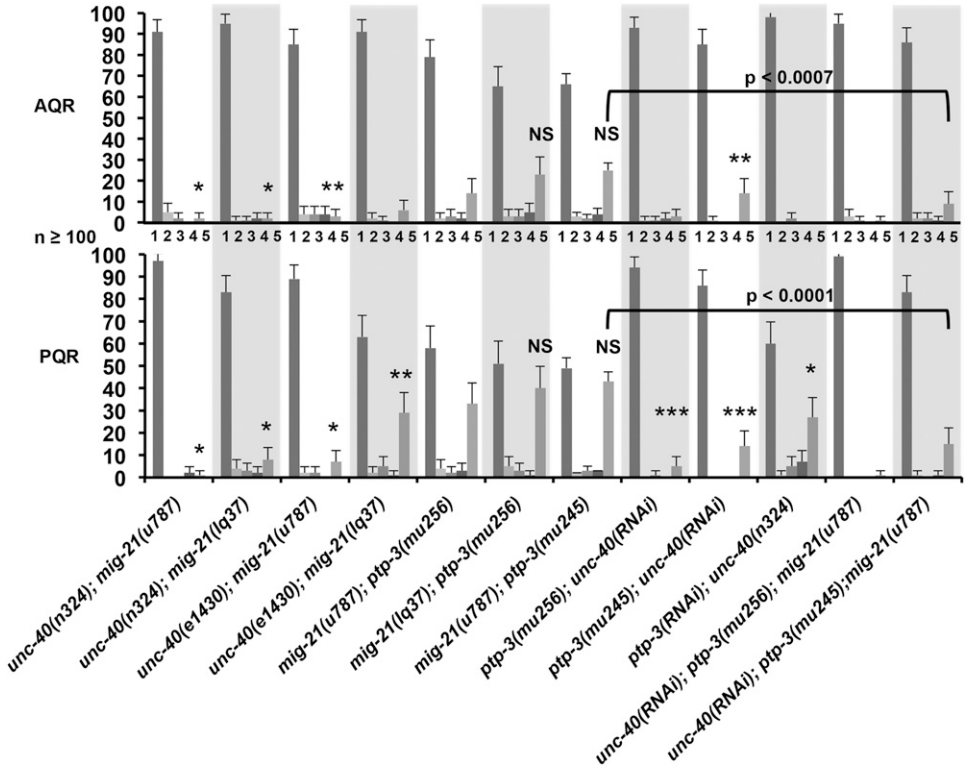

Figure 7 AQR and PQR migration in double and triple mutants. Genotypes are listed on the *x*-axis, and the percentage of AQR and PQR in the five positions along the body axis are shown on the *y*-axis. The five positions (1–5) are described in *Materials and Methods* and Figure 2. Asterisks denote statistical significance compared to single mutant genotypes displayed in Figure 3 as determined by Fisher exact analysis. The table below describes the significance of each asterisk. Error bars represent two times the standard error of the proportion. At least 100 animals were scored for each genotype.

sources cannot be definitively excluded, this result suggests that UNC-40 acts autonomously in the Q cells.

unc-40 RNAi driven by the *scm* promoter enhanced QL/QR and AQR/PQR migration defects of *ptp-3* and *mig-21* (Figure 7), suggesting that UNC-40 acts in the seam cells and/or Q cells. However, RNAi can spread from one tissue to another (systemic RNAi) (Tabara *et al.* 1998; Timmons *et al.* 2001), so it is possible that RNAi expressed from the *scm* promoter might spread to other tissues, and that knockdown in other tissues is responsible for AQR and PQR migration defects. The SID-1 protein is required for spreading of RNAi, as SID-1 affects the ability of cells to accumulate extracellular dsRNA molecules (Winston *et al.* 2002). Previous studies have used transgenic expression of *sid-1* to sensitize neurons to systemic RNAi (Calixto *et al.* 2010). Here, we test whether SID-1 function is required for the effects of cell-specific RNAi expressed by the *scm* promoter. We tested the efficacy of *unc-40(RNAi)* enhancement of *ptp-3(mu256)* in a *sid-1(pk3321)* background and found that AQR and PQR defects were slightly but not significantly reduced compared to the *sid-1 (+)* background (Figure 9). Together with rescue of *unc-40* mutants by the *Pscm*::*unc-40* and *Pegl-17*::*unc-40* construct, these data indicate that UNC-40 acts in the Q cells in AQR and PQR migration.

MIG-21 expression in the Q cells using the *egl-17* promoter rescued defects, indicating that MIG-21 acts autonomously in the Q cells (Middelkoop *et al.* 2012). We were unable to obtain cell-specific rescue of *mig-21* with a transgene containing the *scm* promoter driving the *mig-21(+)* coding region fused to *gfp*, nor could we detect GFP expression. The endogenous expression of *mig-21* is transient in the Q neuroblasts at the time that they are extending protrusions (1–2 hr after hatching) and diminishes rapidly as the cell bodies migrate (Middelkoop *et al.* 2012). Possibly, the *Pscm*::*mig-21*::*gfp* construct is not expressed at the correct time or level to rescue *mig-21* mutants.

We found that *mig-21* RNAi expressed from the *scm* promoter caused AQR and PQR migration defects (Figure 9). Furthermore, *mig-21(RNAi)* significantly enhanced PQR migration defects of *unc-40(n324)*, and *unc-40(n324)* significantly suppressed AQR posterior migration of *mig-21(RNAi)*, similar to *mig-21(u787)* (Figure 9). *unc-40(n324)*; *mig-21 (RNAi)*; *sid-1(pk3321)* mutant AQR and PQR defects were not significantly different from the *sid-1(+)* background (Figure 9), suggesting that *mig-21* knockdown in the seam cells and/or Q cells was causing the defects. This is consistent with previous studies showing cell autonomy of *mig-21* function in the Q cells (Middelkoop *et al.* 2012).

Similar studies were conducted on *ptp-3*. A transgene containing the endogenous *ptp-3B* gene under its own promoter fused to *gfp* (see *Materials and Methods*) rescued AQR and PQR migration defects of *ptp-3(mu256)*, as did expression from the *dpy-7* promoter active in all hypodermis including the seam cells and the early Q cells (Gilleard *et al.* 1997) (Figure 8C). Q-cell–specific *Pegl-17*::*ptp-3B* expression also rescued *ptp-3(mu256)* and *ptp-3(mu245)* AQR and PQR migration defects, suggesting autonomy of *ptp-3* function in the Q cells. However, expression of *ptp-3B*::*gfp* from the *scm* seam cell promoter did not significantly rescue *ptp-3(mu256)* (Figure 8C), despite robust expression of PTP-3B::GFP

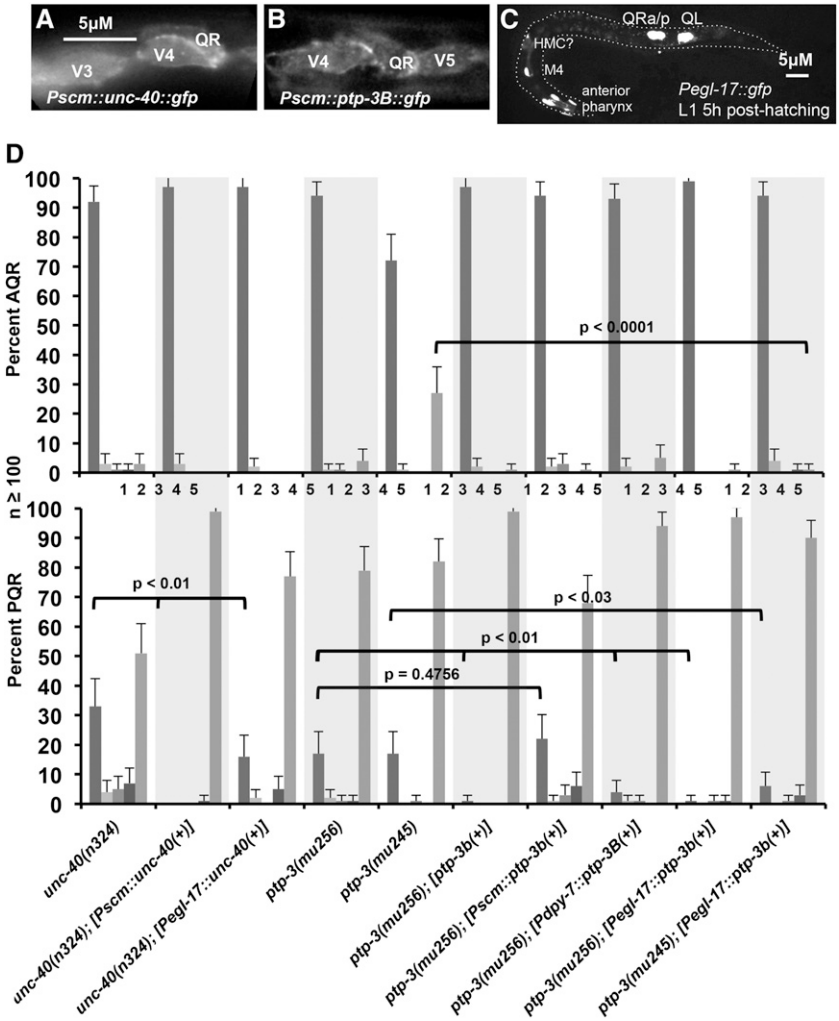

Figure 8 Rescue of AQR and PQR defects using cell-specific transgenes. In all micrographs, anterior is to the left, and dorsal is up. (A) Micrograph showing UNC-40::GFP expression from the *scm*::*unc-40*::*gfp* transgene (*lqIs151*) in seam cells (V3–V5) and QR at 2–2.5 hr after hatching. UNC-40::GFP accumulated at the cell margins. Bar, 5 μM for A and B. (B) Expression of PTP-3B::gfp from the *scm*::*ptp-3B*::*gfp* transgene (*lqEx637*) in the seam cells V4 and V5 and QR at 2–2.5 hr after hatching. PTP-B::gfp accumulated at cell margins similar to UNC-40::GFP. (C) *Pegl-17*::*gfp* expression from the *ayIs9* transgene in an early L1 larva 5 hr after hatching. Q cells have migrated, and QR has divided. In the anterior, expression is observed in some anterior pharyngeal cells, the M4 pharyngeal neuron, and a cell whose position and morphology resemble the head mesodermal cell (HMC). Weak fluorescence along the length of the animal is autofluorescence from the gut. Dashed line indicates the approximate outline of the body of the animal. (D) Graph is shown relating genotypes on the *x*-axis with the percentage of AQR and PQR in the five positions as described in *Materials and Methods* and Figure 2. *[Pscm::unc-40(+)]* is the *Pscm promoter*::*unc-40*::*gfp* transgene *lqIs151*, shown in A; *[ptp-3B(+)]* is the full length *ptp-3B*::*gfp* under its own promoter (*juIs179)*, and *[Pscm*::*ptp-3B(+)]* is the *Pscm*::*ptp-3B*::*gfp* transgene (*lqEx637*) shown in B (see *Materials and Methods*). Statistical significances of difference were determined by Fisher exact analysis, and error bars represent two times the standard error of the proportion.

in the seam and Q cells and cell margin accumulation (Figure 8B). Furthermore, *ptp-3* RNAi driven by the *scm* promoter enhanced PQR migration defects of *unc-40(n324)* but the enhancement was abolished in a *sid-1(pk3321)* mutant background (Figure 9). That *Pegl-17*::*ptp-3B* rescued *ptp-3* mutants argues that *ptp-3* can act cell autonomously, as the *egl-17* promoter was active only in the Q cells in the posterior at the time of initial Q migration (Figure 8C). However, expression in other cells driven by the *egl-17* promoter (pharyngeal cells, the M4 neuron, and later P cell expression) cannot be excluded. Lack of rescue by *Pscm*::*ptp-3B* and *sid-1* sensitivity of *scm* promoter-driven RNAi suggest that *ptp-3* might also have a nonautonomous role in Q cell migration.

Discussion

Previous results showed that MIG-21 and UNC-40 act redundantly in posterior QL migration (Middelkoop *et al.* 2012). Our results presented here confirm this finding in QL and suggest that MIG-21 and UNC-40 might repress each other in posterior QR migration, allowing QR to migrate anteriorly (Figure 9). In the *mig-21*; *unc-40* double null mutant, there was no posterior migration of either QL or QR, consistent with a central role of UNC-40 and MIG-21 in promoting posterior migration. The LAR receptor tyrosine phosphatase PTP-3 has been implicated in Q cell and descendant migration (Williams 2003). We present evidence here that UNC-40 and PTP-3 act redundantly in posterior QL migration, and that MIG-21 and PTP-3 might act in the same pathway in parallel to UNC-40. *unc-40* RNAi knockdown consistently reduced posterior QR migration in *ptp-3*, similar to *unc-40* suppression of this defect in *mig-21*, and *mig-21*; *ptp-3* double mutants showed posterior QR migration similar to either single alone. Thus, MIG-21 and PTP-3 might act in the same pathway in parallel to UNC-40 in Q migration (Figure 10).

The initial protrusion and migration of QL and QR affect the subsequent expression of MAB-5 in the Q descendants and thus their anterior posterior migration (Chapman *et al.* 2008; Middelkoop *et al.* 2012). QR is inherently less sensitive than QL to the EGL-20/Wnt signal that activates MAB-5 expression (Whangbo and Kenyon 1999), and MIG-21 appears to mediate this differential sensitivity (Middelkoop *et al.* 2012). That AQR and PQR defects generally follow the trend of QL

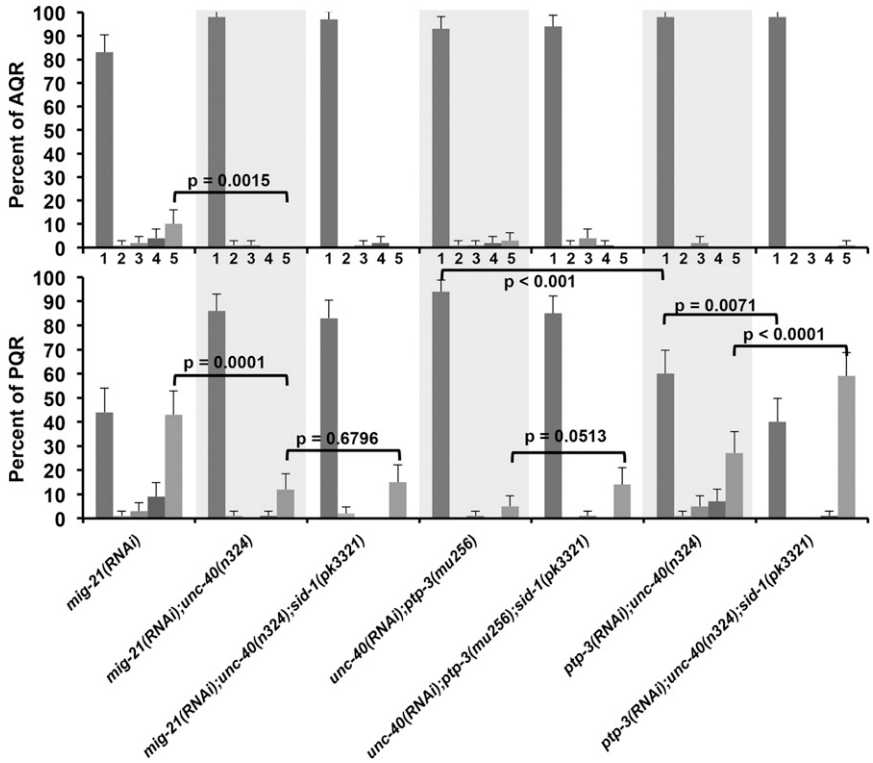

Figure 9 Cell autonomous RNAi of *mig-21*, *unc-40*, and *ptp-3* and the effects of *sid-1(pk3321)*. The *x*-axis shows genotypes analyzed, and the *y*-axis shows the percentage of AQR and PQR cells in each of the five positions as described in *Materials and Methods* and Figure 2. *mig-21(RNAi)* represents the *scm*::*mig-21(RNAi)* transgene *lqEx661*; *unc-40(RNAi)* represents the *scm*::*unc-40(RNAi)* transgene *lqIs146*; and *ptp-3(RNAi)* represents the *scm*::*ptp-3(RNAi)* transgene *lqIs166* (see *Materials and Methods*). Statistical significances of difference were determined by Fisher exact analysis, and error bars represent two times the standard error of the proportion.

and QR migration defects in these mutants is consistent with this idea that initial Q protrusion and migration affects *mab-5* expression and subsequent Q descendant migration.

MIG-21 and UNC-40 mutual inhibition in QR

We found that *unc-40*; *mig-21* double mutants displayed no posterior QR migration, in contrast to each single mutant alone, which showed significant QR posterior migration. This result suggests that UNC-40 and MIG-21 can promote posterior migration in QR as in QL, but in QR they mutually repress each other's activity, allowing anterior migration (Figure 10). In a *mig-21* mutant, UNC-40 was free to promote posterior QR migration; and in an *unc-40* mutant, MIG-21 was free to promote posterior QR migration. Thus, QL and QR have an inherently distinct mechanism involving UNC-40, PTP-3, and MIG-21 to control posterior *vs.* anterior migration. In both QL and QR, these three molecules promote posterior migrations. However, in QR, UNC-40 and MIG-21 repress each other's activity, allowing QR to migrate anteriorly. The nature of this inherent difference in UNC-40 and MIG-21 function in QL *vs.* QR is not understood, but it might be that QL and QR express distinct cytoplasmic molecules that govern this differential action, or that there are differences in the extracellular environments on the left *vs.* the right side, leading to this effect. There is precedence for differences in QL *vs.* QR, as QR is inherently less sensitive than QL to the EGL-20/Wnt signal that induces MAB-5/Hox expression (Whangbo and Kenyon 1999; Middelkoop *et al.* 2012). Indeed, MIG-21 itself is involved in this differential sensitivity to EGL-20/Wnt, positioning MIG-21 as a key regulator of differential responses in initial Q migrations as well as subsequent MAB-5–dependent Q descendant migrations.

While Middelkoop *et al.* (2012) did not address posterior QR migration directly, their data (figure 6A of Middelkoop *et al.* 2012) includes posteriorly directed QR cells in *mig-21 (u787)* mutants (~15–30%), with fewer in *unc-40(e1430)*; *mig-21(u787)* (~0–3%), consistent with our results. They also reported posterior AQR migration in *mig-21(u787)*, which was abolished in *unc-40(e1430)*; *mig-21(u787)*, consistent with our results and with their finding that *unc-40(e1430)*;

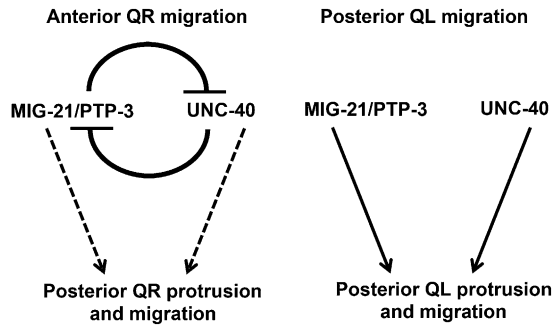

Figure 10 Model of MIG-21, UNC-40, and PTP-3 in Q neuroblast protrusion and migration. (A) Genetic interactions indicate that MIG-21, UNC-40, and PTP-3 are all required for posterior migration. In QL, which normally protrudes and migrates posteriorly, UNC-40 acts in parallel to a pathway involving MIG-21 and PTP-3, as *unc-40* enhanced both *mig-21* and *ptp-3*, but *mig-21* and *ptp-3* did not significantly enhance each other. In QR, which normally protrudes and migrates anteriorly, UNC-40 and a pathway involving MIG-21 and PTP-3 mutually repress each other in QR posterior protrusion and migration, resulting in anterior protrusion and migration. Mutations in one pathway resulted in posterior QR protrusion and migration that was dependent on the function of the other.

mig-21(u787) mutants showed little or no *mab-5* expression due to nearly complete anterior QR and QL migration.

unc-40; ptp-3 embryonic lethality

In our genetic analyses, we found that *unc-40*; *ptp-3* double mutants resulted in embryonic lethality. We did not characterize this lethality here, but *ptp-3* has been shown previously to cause defects in embryonic cell movements in gastrulation resulting in low-penetrance embryonic lethality and to act redundantly with other signaling molecules (*e.g.*, VAB-1/Ephrin) in this process (Harrington *et al.* 2002). Our results indicate that UNC-40 might have a role in gastrulation cell movements in parallel to PTP-3, resulting in embryonic lethality in the double mutant.

Our genetic analysis suggests that *unc-40(e1430)* retains some function and is a hypomorph. PQR migration defects were significantly weaker in *unc-40(e1430)* compared to *unc-40(n324)* and *unc-40(e271)*, and an *n324/e1430 trans*-heterozygote was more severe than *unc-40(e1430)* and resembled *unc-40(n324)* and *unc-40(e271)* homozygotes. While there is no evidence of alternative splicing or alternative exon use in *unc-40*, it is possible that this happens at a low frequency that has not been detected molecularly, leading to functional transcripts in the *unc-40(e1430)* background.

PTP-3/LAR controls Q migration

The LAR receptor protein tyrosine phosphatase PTP-3 was previously implicated in Q migration (Harrington *et al.* 2002; Williams 2003; Ackley *et al.* 2005). We found that *qid-5 (mu245)* (Ch'ng *et al.* 2003) was a new allele of *ptp-3*. *mu245* was a premature stop codon early in the *ptp-3B* coding region (exon 4), which encodes an extracellular portion of the molecule (Figure 1). *mu245* also affects the *ptp-3A*, *D*, and *E* isoforms. However, these isoforms are not relevant to Q migration, as *ptp-3(ok244)*, a deletion that affects these isoforms but not *ptp-3B*, caused no defects in QL, QR, AQR, or PQR migration. Thus, *ptp-3B* is the relevant isoform in Q migration. One caveat is that the shortest *ptp-3C* isoform is not affected by *mu245* or *ok244*, so it is possible that *ptp-3C* also contributes to Q migration.

ptp-3(mu245) mutants were significantly more severe than *ptp-3(mu256)* mutants in QL and QR migration defects, suggesting that *ptp-3(mu256)* is a hypomorph. *ptp-3(mu256)* is a single nucleotide insertion in the coding region for the first intracellular phosphatase domain (Ackley *et al.* 2005), and is predicted to cause frameshifts and premature stops in all known *ptp-3* isoforms, including the shortest *ptp-3C*. It is surprising that a frameshift mutation in a region shared by all isoforms might be a hypomorph. One explanation is that the *ptp-3(mu256)* transcript is subject to nonsense-mediated mRNA decay, affecting all isoforms and functions of the locus. It is also conceivable that the *mu256* insertion is spliced out of some transcripts using cryptic splice sites, or that the intracellular phosphatase domains of PTP-3 are not required for its function in Q migration, and that despite a premature stop codon, some PTP-3 is made in *ptp-3(mu256)*, which lacks the intracellular domains. Consistent with these latter possibilities, *ptp-3(mu256)* animals displayed some anti–PTP-3 immunoreactivity using an antiserum against the entire intracellular region, including the region before the *mu256* insertion (Ackley *et al.* 2005). In photoreceptor axon pathfinding in *Drosophila*, the catalytic activity of the dLAR phosphatase is not required, but the intracellular domains are still required to serve scaffolding functions (Hofmeyer and Treisman 2009).

PTP-3 and MIG-21 might act in the same pathway in parallel to UNC-40

Genetic data presented here suggest that MIG-21 and PTP-3 might act in the same pathway in parallel to UNC-40. The *ptp-3(mu245)* phenotype resembled *mig-21(u787)* in severity QR migration defects compared to *unc-40(n324)* (*ptp-3* and *mig-21* had more severe QR and AQR defects than did *unc-40*), and *mig-21* and *ptp-3* behaved in a similar manner in genetic interactions with *unc-40*. In QL, *unc-40* enhanced both *mig-21* and *ptp-3*, but *ptp-3* did not enhance *mig-21*. Furthermore, *unc-40* reduced posterior QR migration in both *mig-21* and *ptp-3*, and QR posterior migration resembled *ptp-3* and *mig-21* alone in the *ptp-3*; *mig-21* double mutants. Finally, the triple mutant *ptp-3(mu245)*; *mig-21 (u787)*; *unc-40(RNAi)* was not significantly different than the *ptp-3(mu245)*; *unc-40(RNAi)* double mutant. Taken together, these data suggest that PTP-3 and MIG-21 might act together in a pathway in parallel to UNC-40.

UNC-40, PTP-3, and MIG-21 can act autonomously in the Q cells

We found that UNC-40::GFP expressed in the Q cells using the *egl-17* promoter rescued AQR and PQR migration defects of *unc-40(n324)* animals. Furthermore, *unc-40(RNAi)* and *mig-21(RNAi)* expressed by the *scm* promoter enhanced AQR and PQR migration defects similar to *unc-40* and *mig-21* alleles and was not sensitive to *sid-1(pk3321)*. These results suggest that UNC-40 and MIG-21 act autonomously in the Q cells.

Rescue of *ptp*-3 mutants by expression of *ptp-3B* from the *egl-17* promoter active in the Q cells argues that *ptp-3* can act autonomously in the Q cells. However, expression in the Q cells and the seam cells by the *scm* promoter did not rescue. Possibly, the timing or levels of *ptp-3B* expression from the *scm* promoter were not conducive to *ptp-3* rescue. It is also possible transgenic PTP-3B expression on the neighboring seam cells might inhibit PTP-3B function in the Q cells, possibly through a homophilic interaction, suggesting a possible nonautonomous role of PTP-3B. The sensitivity of *scm* promoter driven *ptp-3* RNAi to *sid-1(pk3321)* also hints at a possible nonautonomous role of PTP-3. Thus, the *Pegl-17*::*ptp-3B* rescue experiments argue that *ptp-3* can act autonomously in the Q cells, but *ptp-3* might also have nonautonomous roles as well.

Most known roles of LAR have been shown to be or are presumed to be cell autonomous (for examples, see Srinivasan *et al.* 2012; Wang *et al.* 2012). Our studies indicate that PTP-3B can act autonomously in the Q cells, possibly as a receptor.

However, our data hint that *ptp-3* might also have a nonautonomous role, possibly as a ligand. The transmembrane PTP-3 molecule could play a juxtacrine role, requiring cell–cell contact. It is also possible that the extracellular domain of PTP-3 is cleaved and serves as a diffusible signaling molecule. Indeed, the extracellular domain of mammalian LAR is shed in response to calcium ionophores, phorbol esters, and EGF receptor activity mediated by the alpha-secretase matrix metalloprotease ADAM-17/TACE (Aicher *et al.* 1997; Ruhe *et al.* 2006; Haapasalo *et al.* 2007). These studies show that ectodomain shedding is important for the regulation of the intracellular domain of LAR (an autonomous function), but it is possible that the cleaved ectodomain plays a nonautonomous signaling role.

We envision a mechanism in which UNC-40/DCC, PTP-3/LAR, and MIG-21 act as receptors for an extracellular signal that controls Q migration, and that these molecules interact with each other distinctly in QR *vs.* QL (Figure 10). Our genetic analysis suggests that PTP-3 and MIG-21 are in the same genetic pathway in parallel to UNC-40. It is possible that these molecules interact physically as co-receptors in complexes that regulate responses to anterior–posterior guidance cues.

Many genes have been identified that control early Q neuroblast migrations, yet none encode a molecule that acts nonautonomously as a guidance signal. The transmembrane CUB-domain containing molecule MIG-13 nonautonomously guides Q descendants in the anterior–posterior axis and is present on the commissures of motor axons in an anterior-to-posterior gradient along the animal (Sym *et al.* 1999), but MIG-13 does not affect early Q neuroblast migration. Further studies of genes affecting this process might reveal a signaling molecule that controls Q neuroblast migration via the parallel PTP-3/LAR and UNC-40/DCC pathways.

Acknowledgments

The authors thank B. Ackley, J. Culotti, G. Garriga, and J. Teuliere for plasmids and reagents; O. Hobert, A. Boyanov, and M. Doitsidou for next generation sequencing assistance; S. Macdonald for assistance with TopHat and IGV2.0.15; J. Dyer for assistance with Q neuroblast scoring; E. Struckhoff for technical assistance; and members of the Lundquist and Ackley labs for discussion and critical feedback on this project. Some nematode strains used in this work were provided by the Caenorhabditis Genetics Center, which is funded by the National Institutes of Health (NIH) National Center for Research Resources (NCRR). This work was supported by NIH grants R01NS040945 and R21NS070417 to E.A.L., and NIH grant P20 RR016475 from the Kansas Infrastructure Network for Biomedical Research Excellence program of the NCRR.

Literature Cited

Ackley, B. D., R. J. Harrington, M. L. Hudson, L. Williams, C. J. Kenyon *et al.*, 2005 The two isoforms of the Caenorhabditis elegans leukocyte-common antigen related receptor tyrosine phosphatase PTP-3 function independently in axon guidance and synapse formation. J. Neurosci. 25: 7517–7528.

Aicher, B., M. M. Lerch, T. Muller, J. Schilling, and A. Ullrich, 1997 Cellular redistribution of protein tyrosine phosphatases LAR and PTPsigma by inducible proteolytic processing. J. Cell Biol. 138: 681–696.

Alexander, M., K. K. Chan, A. B. Byrne, G. Selman, T. Lee *et al.*, 2009 An UNC-40 pathway directs postsynaptic membrane extension in Caenorhabditis elegans. Development 136: 911–922.

Bigelow, H., M. Doitsidou, S. Sarin, and O. Hobert, 2009 MAQGene: software to facilitate C. elegans mutant genome sequence analysis. Nat. Methods 6: 549.

Branda, C. S., and M. J. Stern, 2000 Mechanisms controlling sex myoblast migration in Caenorhabditis elegans hermaphrodites. Dev. Biol. 226: 137–151.

Calixto, A., D. Chelur, I. Topalidou, X. Chen, and M. Chalfie, 2010 Enhanced neuronal RNAi in C. elegans using SID-1. Nat. Methods 7: 554–559.

Ch'ng, Q., L. Williams, Y. S. Lie, M. Sym, J. Whangbo *et al.*, 2003 Identification of genes that regulate a left-right asymmetric neuronal migration in *Caenorhabditis elegans*. Genetics 164: 1355–1367.

Chalfie, M., and J. Sulston, 1981 Developmental genetics of the mechanosensory neurons of Caenorhabditis elegans. Dev. Biol. 82: 358–370.

Chalfie, M., J. N. Thomson, and J. E. Sulston, 1983 Induction of neuronal branching in Caenorhabditis elegans. Science 221: 61–63.

Chapman, J. O., H. Li, and E. A. Lundquist, 2008 The MIG-15 NIK kinase acts cell-autonomously in neuroblast polarization and migration in C. elegans. Dev. Biol. 324: 245–257.

Cordes, S., C. A. Frank, and G. Garriga, 2006 The C. elegans MELK ortholog PIG-1 regulates cell size asymmetry and daughter cell fate in asymmetric neuroblast divisions. Development 133: 2747–2756.

Davis, M. W., M. Hammarlund, T. Harrach, P. Hullett, S. Olsen *et al.*, 2005 Rapid single nucleotide polymorphism mapping in C. elegans. BMC Genomics 6: 118.

Du, H., and M. Chalfie, 2001 Genes regulating touch cell development in *Caenorhabditis elegans*. Genetics 158: 197–207.

Dyer, J. O., R. Demarco, and E. A. Lundquist, 2010 Distinct roles of Rac GTPases and the UNC-73/Trio and PIX-1 Rac GTP exchange factors in neuroblast protrusion and migration in C. elegans. Small GTPases 1: 44–61.

Eisenmann, D. M., 2005 Wnt signaling (June 25, 2005), *WormBook*, ed. The *C. elegans* Research Community WormBook, doi/10.1895/wormbook.1.7.1, http://www.wormbook.org.

Esposito, G., E. Di Schiavi, C. Bergamasco, and P. Bazzicalupo, 2007 Efficient and cell specific knock-down of gene function in targeted C. elegans neurons. Gene 395: 170–176.

Gilleard, J. S., J. D. Barry, and I. L. Johnstone, 1997 cis regulatory requirements for hypodermal cell-specific expression of the Caenorhabditis elegans cuticle collagen gene dpy-7. Mol. Cell. Biol. 17: 2301–2311.

Haapasalo, A., D. Y. Kim, B. W. Carey, M. K. Turunen, W. H. Pettingell *et al.*, 2007 Presenilin/gamma-secretase-mediated cleavage regulates association of leukocyte-common antigen-related (LAR) receptor tyrosine phosphatase with beta-catenin. J. Biol. Chem. 282: 9063–9072.

Harrington, R. J., M. J. Gutch, M. O. Hengartner, N. K. Tonks, and A. D. Chisholm, 2002 The C. elegans LAR-like receptor tyrosine phosphatase PTP-3 and the VAB-1 Eph receptor tyrosine kinase have partly redundant functions in morphogenesis. Development 129: 2141–2153.

Harris, J., L. Honigberg, N. Robinson, and C. Kenyon, 1996 Neuronal cell migration in C. elegans: regulation of Hox gene expression and cell position. Development 122: 3117–3131.

Harterink, M., D. H. Kim, T. C. Middelkoop, T. D. Doan, A. van Oudenaarden *et al.*, 2011 Neuroblast migration along the anteroposterior axis of C. elegans is controlled by opposing gradients of Wnts and a secreted Frizzled-related protein. Development 138: 2915–2924.

Hedgecock, E. M., J. G. Culotti, and D. H. Hall, 1990 The *unc-5*, *unc-6*, and *unc-40* genes guide circumferential migrations of pioneer axons and mesodermal cells on the epidermis in *C. elegans*. Neuron 4: 61–85.

Herman, M. A., 2003 Wnt signaling in C. elegans, pp. 187–212 in *Wnt Signaling in Development*, edited by M. Kühl. Landes Biosciences, Georgetown, TX.

Hofmeyer, K., and J. E. Treisman, 2009 The receptor protein tyrosine phosphatase LAR promotes R7 photoreceptor axon targeting by a phosphatase-independent signaling mechanism. Proc. Natl. Acad. Sci. USA 106: 19399–19404.

Honigberg, L., and C. Kenyon, 2000 Establishment of left/right asymmetry in neuroblast migration by UNC-40/DCC, UNC-73/Trio and DPY-19 proteins in C. elegans. Development 127: 4655–4668.

Johnson, K. G., A. P. Tenney, A. Ghose, A. M. Duckworth, M. E. Higashi *et al.*, 2006 The HSPGs Syndecan and Dallylike bind the receptor phosphatase LAR and exert distinct effects on synaptic development. Neuron 49: 517–531.

Keino-Masu, K., M. Masu, L. Hinck, E. D. Leonardo, S. S.-Y. Chan *et al.*, 1996 *Deleted in Colorectal Cancer* (DCC) encodes a netrin receptor. Cell 87: 175–185.

Kenyon, C., 1986 A gene involved in the development of the posterior body region of *C. elegans*. Cell 46: 477–487.

Korswagen, H. C., M. A. Herman, and H. C. Clevers, 2000 Distinct beta-catenins mediate adhesion and signalling functions in C. elegans. Nature 406: 527–532.

Langmead, B., C. Trapnell, M. Pop, and S. L. Salzberg, 2009 Ultrafast and memory-efficient alignment of short DNA sequences to the human genome. Genome Biol. 10: R25.

Levy-Strumpf, N., and J. G. Culotti, 2007 VAB-8, UNC-73 and MIG-2 regulate axon polarity and cell migration functions of UNC-40 in C. elegans. Nat. Neurosci. 10: 161–168.

Mello, C., and A. Fire, 1995 DNA transformation. Methods Cell Biol. 48: 451–482.

Middelkoop, T. C., L. Williams, P. T. Yang, J. Luchtenberg, M. C. Betist *et al.*, 2012 The thrombospondin repeat containing protein MIG-21 controls a left-right asymmetric Wnt signaling response in migrating C. elegans neuroblasts. Dev. Biol. 361: 338–348.

Pan, C. L., J. E. Howell, S. G. Clark, M. Hilliard, S. Cordes *et al.*, 2006 Multiple Wnts and frizzled receptors regulate anteriorly directed cell and growth cone migrations in Caenorhabditis elegans. Dev. Cell 10: 367–377.

Pawson, C., B. A. Eaton, and G. W. Davis, 2008 Formin-dependent synaptic growth: evidence that Dlar signals via Diaphanous to modulate synaptic actin and dynamic pioneer microtubules. J. Neurosci. 28: 11111–11123.

Robinson, J. T., H. Thorvaldsdottir, W. Winckler, M. Guttman, E. S. Lander *et al.*, 2011 Integrative genomics viewer. Nat. Biotechnol. 29: 24–26.

Ruhe, J. E., S. Streit, S. Hart, and A. Ullrich, 2006 EGFR signaling leads to downregulation of PTP-LAR via TACE-mediated proteolytic processing. Cell. Signal. 18: 1515–1527.

Salser, S. J., and C. Kenyon, 1992 Activation of a C. elegans Antennapedia homologue in migrating cells controls their direction of migration. Nature 355: 255–258.

Srinivasan, S., A. P. Mahowald, and M. T. Fuller, 2012 The receptor tyrosine phosphatase Lar regulates adhesion between Drosophila male germline stem cells and the niche. Development 139: 1381–1390.

Sulston, J., and J. Hodgkin, 1988 Methods, pp. 587–606 in *The Nematode Caenorhabditis elegans*, edited by W. B. Wood. Cold Spring Harbor Laboratory Press, Cold Spring Harbor, NY.

Sulston, J. E., and H. R. Horvitz, 1977 Post-embryonic cell lineages of the nematode, Caenorhabditis elegans. Dev. Biol. 56: 110–156.

Sym, M., N. Robinson, and C. Kenyon, 1999 MIG-13 positions migrating cells along the anteroposterior body axis of C. elegans. Cell 98: 25–36.

Tabara, H., A. Grishok, and C. C. Mello, 1998 RNAi in C. elegans: soaking in the genome sequence. Science 282: 430–431.

Terns, R. M., P. Kroll-Conner, J. Zhu, S. Chung, and J. H. Rothman, 1997 A deficiency screen for zygotic loci required for establishment and patterning of the epidermis in Caenorhabditis elegans. Genetics 146: 185–206.

Thorvaldsdottir, H., J. T. Robinson, and J. P. Mesirov, 2012 Integrative Genomics Viewer (IGV): high-performance genomics data visualization and exploration. Brief. Bioinform. (in press).

Timmons, L., D. L. Court, and A. Fire, 2001 Ingestion of bacterially expressed dsRNAs can produce specific and potent genetic interference in Caenorhabditis elegans. Gene 263: 103–112.

Wang, F., S. N. Wolfson, A. Gharib, and A. Sagasti, 2012 LAR receptor tyrosine phosphatases and HSPGs guide peripheral sensory axons to the skin. Curr. Biol. 22: 373–382.

Whangbo, J., and C. Kenyon, 1999 A Wnt signaling system that specifies two patterns of cell migration in C. elegans. Mol. Cell 4: 851–858.

White, J. G., E. Southgate, J. N. Thomson, and S. Brenner, 1986 The structure of the nervous system of the nematode *Caenorhabditis elegans*. Philos. Trans. R. Soc. Lond. 314: 1–340.

Williams, L., 2003 A genetic analysis of the left-right asymmetric polarizations and migrations of the Q neuroblasts in C. elegans. Ph.D. Thesis, University of California, San Francisco.

Winston, W. M., C. Molodowitch, and C. P. Hunter, 2002 Systemic RNAi in C. elegans requires the putative transmembrane protein SID-1. Science 295: 2456–2459.

Zinovyeva, A. Y., Y. Yamamoto, H. Sawa, and W. C. Forrester, 2008 Complex network of Wnt signaling regulates neuronal migrations During Caenorhabditis elegans. Dev. Genet. 179: 1357–1371.

Communicating editor: K. Kemphues

GENETICS

Supporting Information
http://www.genetics.org/lookup/suppl/doi:10.1534/genetics.112.145706/-/DC1/

Transmembrane Proteins UNC-40/DCC, PTP-3/LAR, and MIG-21 Control Anterior–Posterior Neuroblast Migration with Left–Right Functional Asymmetry in *Caenorhabditis elegans*

Lakshmi Sundararajan and Erik A. Lundquist

DOI: 10.1534/genetics.112.145706

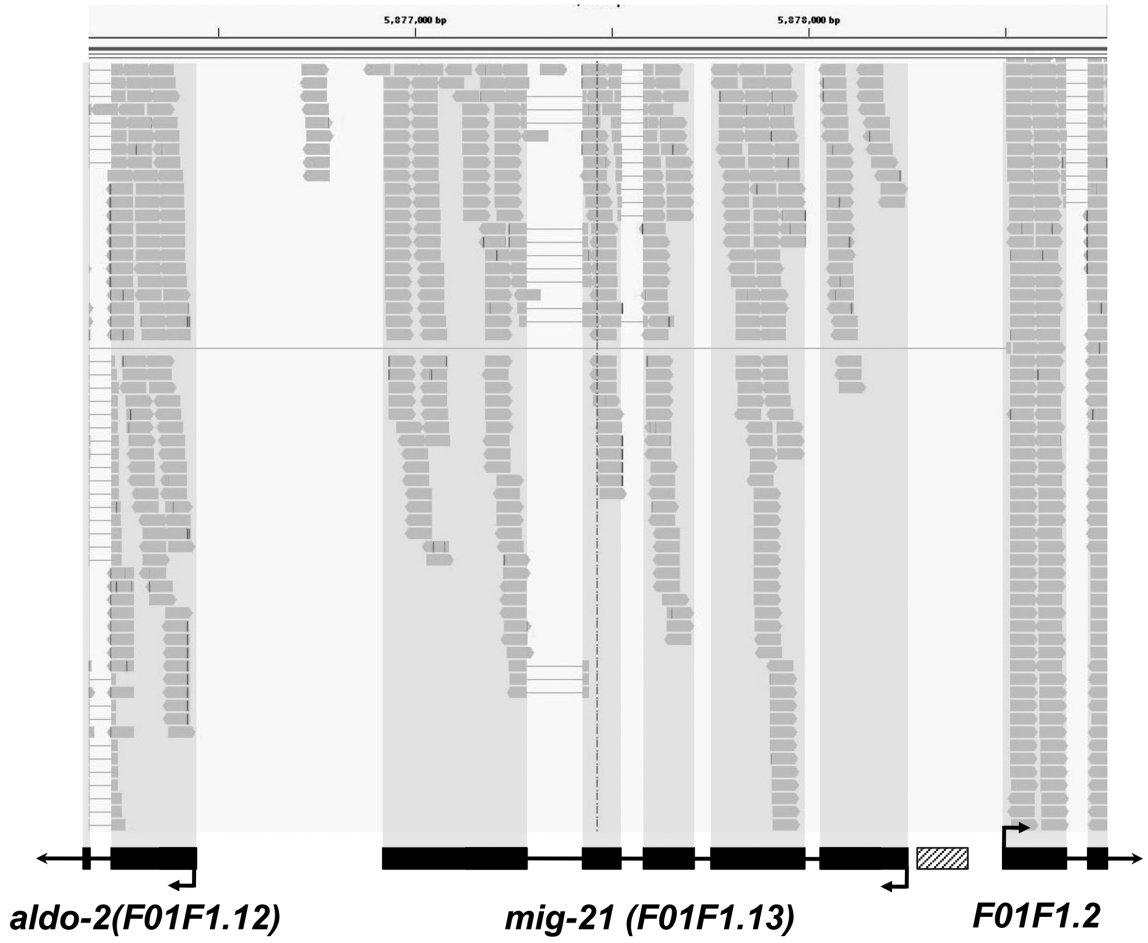

Figure S1 The *mig-21* locus as defined by RNA seq transcript sequencing. Shown is output from the Integrated Genome Viewer 2.0.15 program which aligned RNA seq reads (grey bars) from L1 larvae at 5-5.5 h post hatching to the *C. elegans* genome. The *F01F1.13/mig-21* region is shown, as are the flanking genes *F01F1.12/aldo-1* and *F01F1.2*. Read polarity is indicated by a point at the end of each run, and thin lines between reads indicate that the read aligned across a putative intron. The hatched box represents the region of exon 1 predicted in Middelkoop et al., 2012 but that is not represented by reads in this RNA seq analysis.

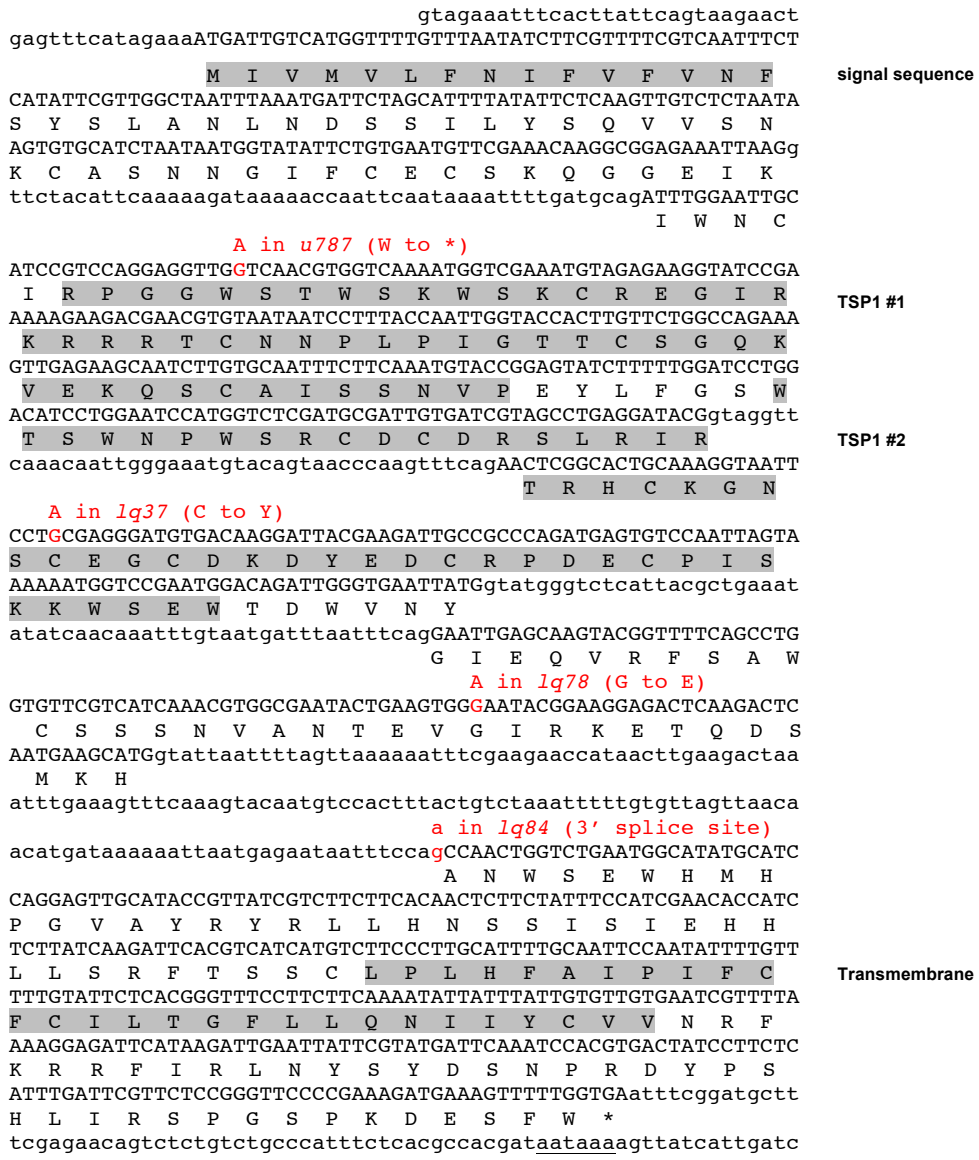

Figure S2 The *mig-21* coding region. The DNA sequence of the *mig-21* coding region as determined from cDNAs and transcript sequencing runs on Wormbase, and from our RNA seq analysis. The predicted 5' and 3' untranslated regions and introns are lowercase, and the open reading frame is upper case. A putative poly-A site in the 3' UTR is underlined. Nucleotide lesions associated with *mig-21* alleles are shown in red above the DNA sequence. The putative polypeptide encoded by *mig-21* is shown below the DNA sequence. A potential signal sequence, two potential thrombospondin type I domains, and a potential transmembrane domain and highlighted in grey.

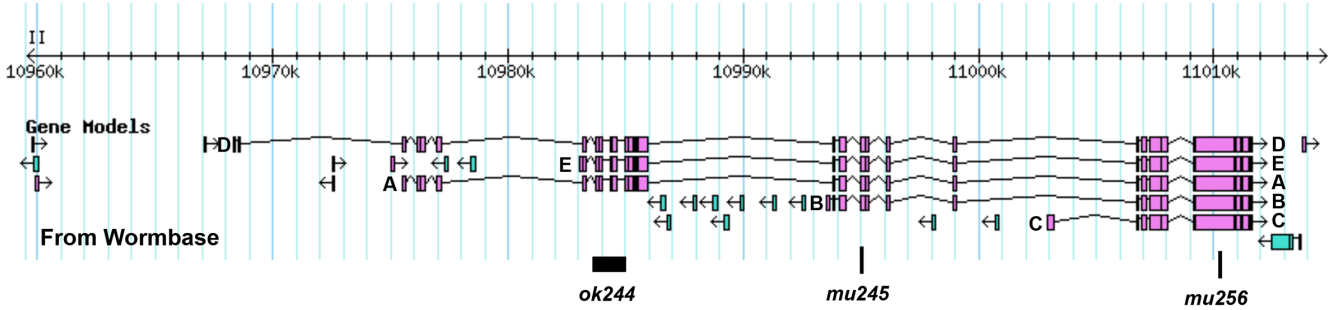

mu245: ***ptp*-3B exon 4** **A**

ACAATCTATGGTTACGCGCACAAGGATATCCGGACTCATATGTCAAGGCGAAGACAGTCGACGGAACCGATCTATCAAC

mu256: ***ptp*-3B exon 12** **GA**

CTGCCACATATGGAGATATCGAGGTGACACTGTTGGAAAGCGTTCATTTGGCTCATTATACGATGAGAACGATGCGATT

Figure S3 The *ptp-3* locus and mutations. A screen shot from Wormbase 229 of the *ptp-3* locus with the A-E isoforms indicated. The sites of *ptp-3* mutations are shown, with the corresponding nucleotide changes below.

Table S1 Data for Q protrusion and migration in mutants. The table contains data for QR and QL protrusion and migration at three stages: 2-2.5 hours post-hatch when the Q cells have protruded; 3-3.5 h post hatch when the Q cells have migrated; and 4-4.5 h post hatch, when the Q cells have undergone their first division.

Available for download at http://www.genetics.org/lookup/suppl/doi:10.1534/genetics.112.145706/-/DC1/.